The Dissertation Committee for Thomas Eugene Kreschollek Certifies that this is the approved version of the following dissertation:

Multiplexed Carbon Braid ETV and Tandem ETV-Nebulizer Sample Introduction for ICPMS

Committee:

James A. Holcombe, Supervisor

Jennifer S. Brodbelt

Todd B. Housh

David A. Laude

David A. Vandenbout

Multiplexed Carbon Braid ETV and Tandem ETV-Nebulizer Sample Introduction for ICPMS

by

Thomas Eugene Kreschollek, B.S.

Dissertation

Presented to the Faculty of the Graduate School of

The University of Texas at Austin

in Partial Fulfillment

of the Requirements

for the Degree of

Doctor of Philosophy

The University of Texas at Austin

May 2007

Dedication

To my dearest Whitney, the friend that showed me the joys of slow walks, been my muse in times of needs and makes the world better for having been touched by you.

Acknowledgements

First and foremost, I want to thank my advisor Dr. Holcombe for the countless number of hours you have helped me when I needed it, and tolerated me when I would not ask for help. I'll miss the long brainstorming sessions that always compared the problem at hand to an electrical circuit. Sometimes I felt we were sparring, but in the end I feel that the lessons were much better learned. I was even lucky to be correct a few times! Thanks fer fix all my papars so that everybody think I spek gud English. I've enjoyed working with you and might be able to call you Jim someday.

Bradley "A." Rowland my attorney and utter opposite. The Dr. Gonzo to my Dr. Duke. The white to my black. The apple to my monkey. The rabid wildebeest to my...you get the point! While you still do not know the difference between resolution and detection limits and I still can't do a triple integral in my head or for fun. For all the great times interacting with the knowledgeable and astute employees of fine vendors of quality wares and goods (*e.g.*, Wal*Mart and Best Buy) and for all the times my stomach hurt from laughing non-stop, I want to thank you. You have been a great friend and have made my short stay in Austin quite enjoyable.

Bill "Bilby" "Rainman" Balsanek. I watched you evolve from pure hedonism to settled family man. It's still strange to think back on the days when I had to make a list of your 'dates' to keep all the names straight. You have a carefree way about you that

sometimes I wish I could have. Other times it makes me want to strangle you. Now to be serious...

Brianna Rose White. One of the greatest scientific minds I have ever encountered. You are a free-thinker that has a base of knowledge that is completely unbounded, touching on a variety of topics in science and engineering. On a personal note, you are a continuing source of inspiration for all of us.

Carina N. Gundar. Your hard working and commitment is a continuing inspiration. Your bright, attentive and thoughtful discussions in group meeting were what made those meetings such a success.

Adam “Gerb” Rowland. Your unbounded energy helped to make the lab run smoothly and safely. I could always count on you make sure we had Ar. I was always comforted by seeing you decked out in the heavy gloves, double disposable gloved, goggles, lab coat and a tube of calcium glutamate sticking out of your pocket whenever you touched HF. You were even dedicated enough to have a tube at home! I can only hope we can all live up to your standard for safety.

Multiplexed Carbon Braid ETV and Tandem ETV-Nebulizer Sample Introduction for ICPMS

Publication No._____

Thomas Eugene Kreschollek, Ph.D

The University of Texas at Austin, 2007

Supervisor: James A. Holcombe

This research focuses on electrothermal vaporization (ETV) as a sample introduction source for inductively coupled plasma mass spectrometry (ICPMS). ETV creates a dry plasma that causes problems when used at the high applied powers (*e.g.,* 1.2 kW) typically employed for nebulizer-based sample introduction for certain ICPMS instruments. A secondary discharge forms in the sampling region of the spectrometer, but this effect was removed by reducing the applied power (*e.g.,* 0.7 kW). A novel, steady state, dry aerosol introduction system was developed to permit optimization of the ICPMS settings. The device used solid NbF_5, $SnBr_4$ and a W filament plated with Pb to generate dry aerosols which produced $^{28}Si^+$, $^{79}Br^+$, $^{120}Sn^+$, $^{184}W^+$, and $^{208}Pb^+$ that were used to optimize the ICPMS. When compared to an ICPMS optimized using a nebulizer, the dry optimized plasma produced an average enhancement of 4.5(±0.4) for 26 elements when using ETV sample introduction.

The ETV produces a short (0.5-2 s) transient pulse once every 2-3 min, resulting in a sample throughput of 20-30 samples/h. To increase this throughput, a low power,

low background multiplexed ETV device using carbon braids as vaporizers was developed. Oxygen ashing was demonstrated with recoveries of 96±17% for a suite of elements. Refractory elements (*e.g.*, V and U) showed precision of greater than 25% while medium to high volatility elements were in the 10-20% range. The lifetime of the braids was limited to *ca.* 30 vaporizations when heated to 2,800ºC.

A device for coupling an ETV in parallel with a nebulizer was also designed and characterized. The device was designed to minimize the impact of the ETV's presence on nebulizer-based ICPMS performance. The ETV could be easily switched on line to provide complimentary information that may be unavailable with nebulizer sample introduction because of isobaric interference problems. For example, in a 1% HCl matrix, the detection limits for $^{51}V^{+}$ ($^{51}ClO^{+}$ interference), $^{75}As^{+}$ ($^{75}ArO^{+}$ interference) and $^{78}Se^{+}$ were found to be 0.008 ppb, 0.088 ppb, 0.063 ppb, respectively. By contrast, the nebulizer detection limits in 1% HCl for $^{51}V^{+}$, ^{75}As and ^{78}Se were found to be 0.593 ppb 1.488 ppb and 1.158 ppb, respectively.

Table of Contents

List of Tables

List of Figures

Chapter 1: Introduction

1.1 Inductively Coupled Plasma for use in elemental Analysis

Inductively coupled plasmas (ICP) have been used profusely in analytical atomic spectroscopy since the first atomic emission system was introduced in 1974[1]. Plasma discharges have been used in atomic emission spectroscopy (AES), hollow cathode lamp atomic fluorescence spectroscopy (HCL-AFS), atomic absorption spectroscopy (AAS) and mass spectrometry (MS). ICP has trumped direct current plasmas (DCP) and microwave-induced plasmas (MIP) due to geometry, stability and robustness of the plasma discharge. The annular shape of the ICP plasma discharge allows samples to interact with the core of the plasma, which was a contrast to MIP and DCP. In ICPMS, the ICP torch is used as an ion source that is interfaced to the mass spectrometer (MS). In this way, the ICP and MS can be considered as separate entities.

1.1.1 Characteristics of an atmospheric-pressure inductively coupled plasma

A plasma is collection of electrons, ions and neutral atoms that is electrically neutral. However, ICP plasmas have been noted to carry a potential, which cause secondary discharge if steps are not taken to mitigate the potential [2-6]. These steps have included guard electrodes[4] and changes in induction coil design[5]. Plasmas exhibit properties that are much different from other forms of matter, because of which the case can be made that plasmas are a fourth state of matter. These properties include: high electrical conductivity, response to electric fields, and production of magnetic fields.

The electron density in an ICP plasma is also high ($1\text{-}3x10^{15}/cm^3$) which reduces ionization-type inferences from forming in ICP plasmas. ICP plasmas have high gas temperatures (4,500 to 8,000 K) and high electron temperature (8,000 to 10,000 K).

Electron temperatures are much higher than the gas temperatures in a plasma because energy is easily imparted into the lighter electrons than the heavier ions in the oscillating magnetic field produced by the induction or load coil (see Figure 1.1). The high temperatures of the plasma and a long sample resonance time (2-3 ms) generally allows for complete desolvation, vaporization and atomization of sample introduced to the plasma. Most metals are >90% ionized in an Ar plasma, making it an excellent ionization source for mass spectrometry. The high temperatures lead to the plasma acting as the extreme of hard ionization sources by dissociating most molecular species[7].

The formation of an argon inductively coupled plasma, which are used in a majority of ICP instruments, requires a few basic components: an induction coil, a torch, suitable plasma gas and seed electrons. The three concentric tubes of the Fassel-type ICP torch, as seen in Figure 1.1, and the three independently controlled gas flows are used to create the plasma.

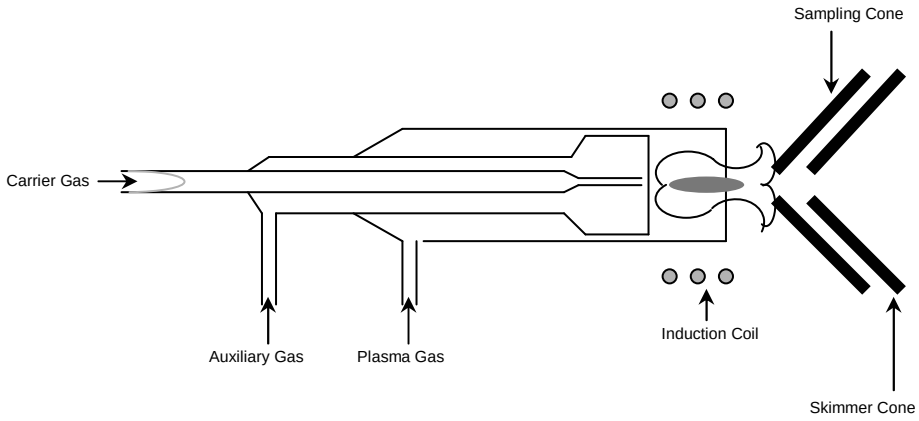

Figure 1.1: Schematic view of Fassel-type ICP torch, induction coil and mass spectrometer interface

The Fassel-type torch is a lower flow (12-18 L/min)[8] torch design that is used with the majority of ICP instruments[9]. The plasma gas flow (10-15 L/min) is the main supply of gas for the plasma. The auxiliary flow (1-1.5 L/min) is introduced tangentially

to pull the plasma away from the quartz torch to prevent melting and move the position of the plasma inside of the torch. The changes in position move the plasma closer or further from the injector tube, which is used to introduce the analyte to the plasma. The analyte is transported via a carrier gas (1 – 1.5 L/min), this cold, dense gas punches a center channel through the plasma to facilitate entrance of the sample aerosol into the plasma. Encircling the plasma, external to the torch, is the induction or load coil.

The induction coil, usually a few turns of gold plated copper tubing, is powered by a 1 – 2 kW radio frequency (RF) generator. Plating the Cu induction coil is important because higher frequency signals travel closer to the surface of the conductor, this is known as the "skin effect".

$$d = \sqrt{\frac{2\rho}{\omega\mu}} \qquad (1.1)$$

where

d = skin depth where current falls to 1/e of current at surface

ρ = resistivity of conductor

ω = angular frequency of current = $2\pi \times$ frequency

μ = absolute magnetic permeability of conductor

Copper oxides, which form readily in air, are poor electrical conductors and thus attenuate the applied RF power. Gold is chemically stable and an excellent electrical conductor, making it an excellent choice for protective plating. The coil geometry can take many forms, each with advantages and disadvantages[9].

In the United States the use of radio frequency devices is regulated by the Federal Communication Commission (FCC) who determines the frequencies that are allotted for specific purposes. The FCC has allocated bandwidth in the electromagnetic spectrum for

industrial, scientific, and medical (ISM) equipment that allows for license-free use with no limit on applied power. To comply with these rules, ICP RF generators are limited to 27.12 MHz or 40.68 MHz[10]. Since the RF generator must operate at a set frequency, the induction coil circuit requires an impedance matching device to allow the maximum amount of energy to be coupled to the gas that forms the plasma. At a particular frequency, when the impendence is minimized, and the maximum amount of current can flow, the circuit is in *resonance*. A tuned circuit resonates at a particular frequency for a given circuit inductance and capacitance. If any of these values change, the conditions in the circuit must change in order to return the circuit to resonance. To be compliant with FCC regulations, the ICP RF source must remain at a fixed frequency requiring the inductance of the load coil to change as the conditions in the core of the coil change. For an ICP, before the plasma is ignited, the power circuit can be tuned to resonate under those conditions. Neutral argon gas is an insulator at room temperature and pressure, with dielectric properties similar to air[11], which gives the unlit torch and load coil a lower inductance. This cool, insulting, uncharged gas requires a much different set of conditions than those that are found when the plasma is lit. Variable, or tunable, capacitors can be used to dynamically change the capacitance of the circuit as conditions demand.

With a resonant circuit that can be retuned to resonance on demand the system is ready to form a plasma. When RF power is applied to the load coil, an oscillating magnetic field is created along the axis of the gas flow. To begin the process needed to form a plasma, seed electrons are added to the Ar gas from an electrical discharge. A Tesla Coil, a type of high voltage disruptive discharge coil, is used to seed the Ar stream with extra electrons. These electrons are accelerated in the magnetic field, and collide with neutral Ar gas, liberating electrons, ionizing the gas and transferring kinetic energy

to form a plasma. When the plasma is formed, the inductance of the load coil changes due to the drop in impedance in the core. This results in an impedance mismatch in the load circuit connected to the RF generator. The tunable capacitors in the load circuit must then be adjusted in order to reestablish resonance.

The primary analytical uses of an ICP are as an ionization source for mass spectrometry (ICPMS), as an excitation source for atomic emission (ICPAES) and as an atom and ion source for atomic fluorescence (ICPAFS). ICPAFS requires the use of a hollow cathode lamp, electrodeless discharge lamp, laser or other suitable high intensity source to act as an excitation source. ICPAFS is a less commonly used technique due to limitations in sensitivity, excessive costs and/or analytical convenience [7].

Detection limits for ICPAES are usually in the 1-100 ppb range for many metals, which is several orders of magnitude above the detection limits of ICPMS[9]. Several elements (*e.g.* Ca) have superior detection limits in ICPAES than in ICPMS due to the argide interferences that are found in ICPMS. However, ICPAES does have its own set of interferences, mainly from spectral overlap. The cost of ICPAES is much less than ICPMS, making it attractive for many applications.[7]

1.1.2 Fundamentals of interfacing an atmospheric inductively coupled plasma as an ion source to a mass spectrometer

The coupling of the atmospheric pressure ICP source to a mass spectrometer that requires sub-Torr pressure presents a challenge. For efficient MS operation, pressures as low as 10^6 Torr are required which are not directly compatible with the atmospheric pressure ICP ion source. To reduce the pressure, a series of cones are used to sample the plasma allowing differential pumping of multiple pressure regions. As shown in Figure 1.1, the plasma is sampled by the sampling cone, behind which the pressure is reduced.

The low density plasma acts to plug the hole of the sampling cone, only allowing a small amount of hot, low density gas into the first vacuum region. The sampling cone is typically nickel or platinum with a ca. 1 mm diameter hole at the apex. The plasma is sampled by the sampling cone, removing only a small fraction of the total gas and expanded in the vacuum region. This expanded gas is then sampled by the skimmer cone for a further reduction in gas load.

The region between the sampling and skimmer cone has a pressure of ca 1-3 Torr; this is then further reduced to ~10^{-6} Torr behind the skimmer cone in the mass analyzer region. Many instruments use a two cone system (one sampling cone and one skimming cone); however, other configurations are possible[12]. Past the interfacing cones, electrostatic lenses are used to shape and steer the ion beam for optimal measurement in the mass spectrometer. The shape of the beam is dictated by the type of mass analyzer that is used.

Many types of mass spectrometers have been coupled to ICP torches in the past. These include quadruples, time-of-flight (TOF), sector field, and ion cyclotron resonance. The vast majority of the mass spectrometers in service and sold in the world today are quadrupole mass spectrometers. Quadrupole mass filters operate by filtering out all m/z other than the one of interest. These filters are popular because of the low initial cost, ruggedness and reasonable m/z scanning rate. However, there are some disadvantages to a quadrupole as well. These include low resolution and potential problems with transient signals. Although unit mass resolution is generally sufficient for atomic mass spectrometry, it doesn't permit isobaric separations. The problems with transient signals arise from the sequential scanning nature of the analyzer. Thus, for transients that are short relative to the individual m/z measurement period ("dwell"), an insufficient number of measurements might be taken for all the masses monitored over the lifetime of the

analytical signals. This has been theoretically discussed[13], and upper limits on monitored masses, precision and accuracy presented [14, 15]. The "spectral skewing" [16] can present its most significant problems if accurate isotopic ratios are sought. For steady state signals these problems can be minimized by long integration times which improve the duty cycle and minimize some of the flicker noise. [15].

1.1.2.1 Digression on Time of Flight Mass Spectrometers

In recent years, time-of-flight (TOF) mass spectrometers have improved their analytical figures of merit so that they are comparable with those of quadrupoles mass filters. Some advantages of the TOF mass spectrometer are the quasi-simultaneous sampling and analysis of the entire mass range with no loss in duty cycle relative to that available for TOF's single ion monitoring. The simultaneous sampling of the plasma minimizes the effects of plasma noise (especially flicker noise) and better compatibility with transient signals. Flicker noise is removed by sampling a "packet" of ions that had experienced the same plasma conditions (see Figure 1.2). The duty cycle for a time-of-flight instrument is fixed, since it will separate all of the analytes in a sample packet, independent of the number of masses that are ultimately monitored. The duty cycle of a quadrupole can be calculated with the following formula.

$$\frac{t_d}{t_s} = \frac{t_d}{t_f + n_m t_d + t_j (n_m - 1)} \qquad (1.2)$$

Where:

t_s= scan time

t_f= flyback time

n_m= number of masses

t_d= dwell time

t_j= jump time

When only a small number of analytes are analyzed, the time-of-flight is at a disadvantage by have a static duty cycle. However, time-of-flight instruments gain an advantage by not losing duty cycle when a large number of m/z values are analyzed, as can be seen in Figure 1.2[17].

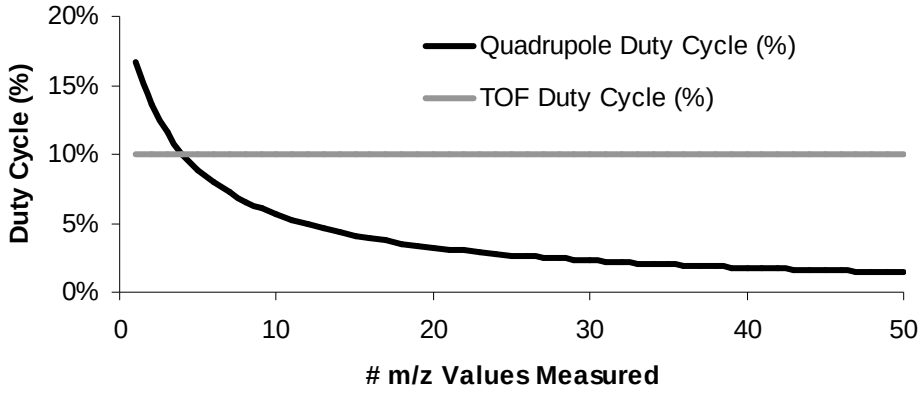

Figure 1.2: Comparison of the static duty cycle of the time of flight mass spectrometer and a quadrupole mass spectrometer as a function of the number of masses monitored.

. Previous work has shown up to 11 m/z values for a transient signal from an electrothermal vaporizer on a quadrupole instrument can be monitored without detriment to precision or accuracy[14] or up to 21 with predictable precision [15] Many factors went into this, including the duration of the transient and the model of the instrument.

The instrument used in this study is a GBC Optimass 8000, an ICP-TOF. A block diagram of this instrument with its orthogonal accelerator is shown in Figure 1.3

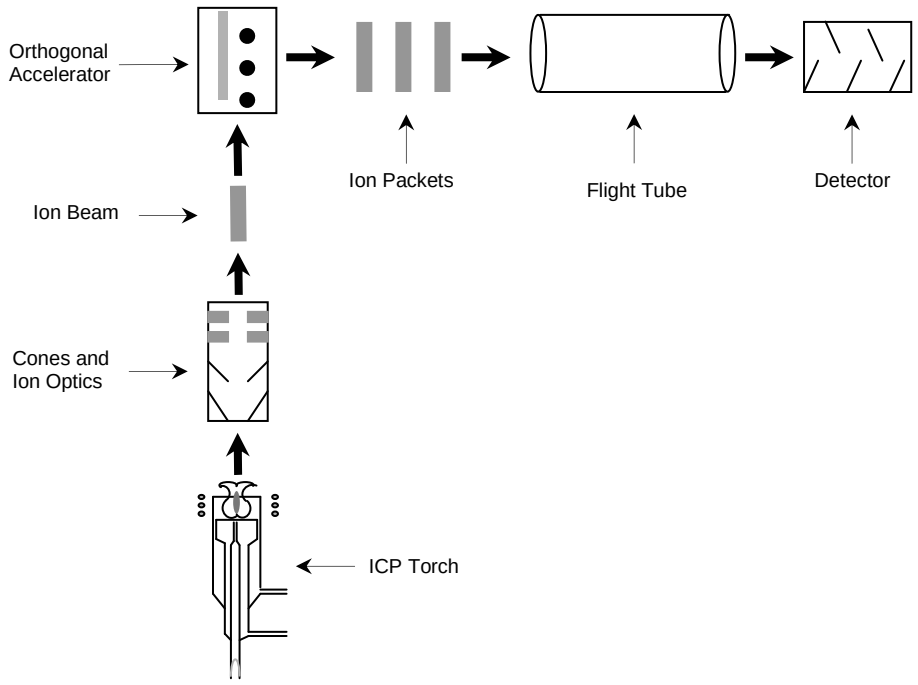

Figure 1.3: Schematic view of an orthogonally accelerated ICP(TOF)MS.

The ion beam originating in the ICP torch travels to the orthogonal accelerator (OA) which uses a pulsed electric field of ca. 200 V orthogonal to the axis of travel to introduce the positive ion packet to the drift region. The OA consists of a plate and grid onto which a square wave pulse is applied to push ions into the flight tube. To a first approximation, the ions are given approximately the same amount of kinetic energy (KE) and separate in the field free drift tube by their mass. The amount of KE imparted will be a product of the ion's charge (z) the electric field in the accelerator (E) and the distance traveled in the field (s_a). This is also equivalent to the KE equation using the mass (m) and velocity (v) of an object to yield the equation:

$$Ezs=1/2mv^2 \quad (1.3)$$

This equation can be rearranged, since v is the product of the distance traveled (D) in a certain amount of time (t_D), to solve for transit time to the detector:

$$t_D = D\sqrt{\frac{m}{2qEs_a}} \qquad (1.4)$$

Given a fixed geometry and applied field, the time required to traverse the flight tube and strike the detector is dependent only on the mass-to-charge ratio. In this instrument the usual flight time for the heaviest mass is ca. 30 μs, which is the minimum time delay between OA pulses or "pushouts" to ensure that all of the ions have cleared the flight tube before the next packet is sent to the detector.

1.2 SAMPLE INTRODUCTION USING ELECTROTHERMAL VAPORIZATION

The principle for using an electrothermal vaporization (ETV) device as a sample introduction tool can be quite simple: After a small amount of sample is introduced onto the ETV, the device is heated to low temperature (ca. 80 ºC) to evaporate the solvent, the temperature is raised slightly (~200-300 ºC) to more fully remove adsorbed solvent, and finally the ETV is pulse heated (ca. 500-2000 ºC/s) to vaporize the sample. Tubular shaped furnaces are the predominate geometry of electrothermal vaporizers. This design evolves directly from the designs used as electrothermal *atomizers* for atomic absorption spectrometry. A variety of other options including metal strips, filaments and wires have also been employed[18].

1.2.1 Background on Electrothermal Vaporization

Electrothermal vaporizers have been used in atomic spectroscopy in many roles. In atomic absorption and atomic fluorescence, the vaporizer is used as an *atomizer, i.e., a* source for the production of free gas phase atoms. The first attempt to use an ETV sample introduction device was made in 1975[19]. Since then, the role of ETVs as a sample introduction tool and the various design options have been regularly explored and the development of ETVs recently reviewed[20]

The benefits of an ETV for plasma techniques lies in the ability of the electrothermal vaporizer to dry (remove solvent) and char/ash (*i.e.*, remove volatile matrix by evaporation or combust organic material using oxygen) the sample before an attempt is made to introduce the analyte into the plasma during the ETV's vaporization stage.

As noted earlier, ETVs have taken on many forms and materials. Cups, rods, tubes, filaments and braids are a few of the design variations, and refractory metals (*e.g.* W, Ta and Re) and graphite represent the dominant materials that have been employed. The analytical, physical and electrical properties of a vaporizer dictate the material and style of the vaporizer. One potential disadvantage of using an ETV for introduction is that the he vaporizer material will usually be introduced to the ICP in significant amounts and can appear as spectral interferences (*e.g.*, W^+, WO^+, C^+, CO^+, etc.) or in combination with analyte ions (*e.g.*, MC^+). These potentially interfering ions can also include impurities in the vaporizer which may limit detection limits if these elements are also sought in the sample. Graphite possess features that made it the material of choice for ETAs, *viz.*, it can be easily purged of metals to high levels of purity, it is capable of reaching high temperatures, chemical inertness and surface oxides that can be easily volatilized. The most commonly used ETV design is the graphite tube-type furnace, in-lab fabricated ETVs and commercial units that have been sold are generally simple adaptations of the graphite tube atomizers used with atomic absorption applications.

Graphite tube-type furnaces, as used in graphite furnace atomic absorption, require 2-5 kW of power in order to heat the device to ca. 3,000 ˚C temperature, which will vaporize most metals. For this design relatively large currents are required due to the relatively low resistance of the graphite tube. These relatively large power requirements are needed to permit fast thermal ramps to the final hold temperatures. Once the final

temperature is reached, significantly smaller powers are needed to hold the furnace at the desired temperature. Unlike most metals, graphite has a negative temperature coefficient of resistivity, which exacerbates the current requirements as the furnace heats. Thus, high current (300-600 A) and low voltage (6-10 V) power supplies are generally employed. [21].

A schematic view of a side streaming ETV is pictured in Figure 1.4.

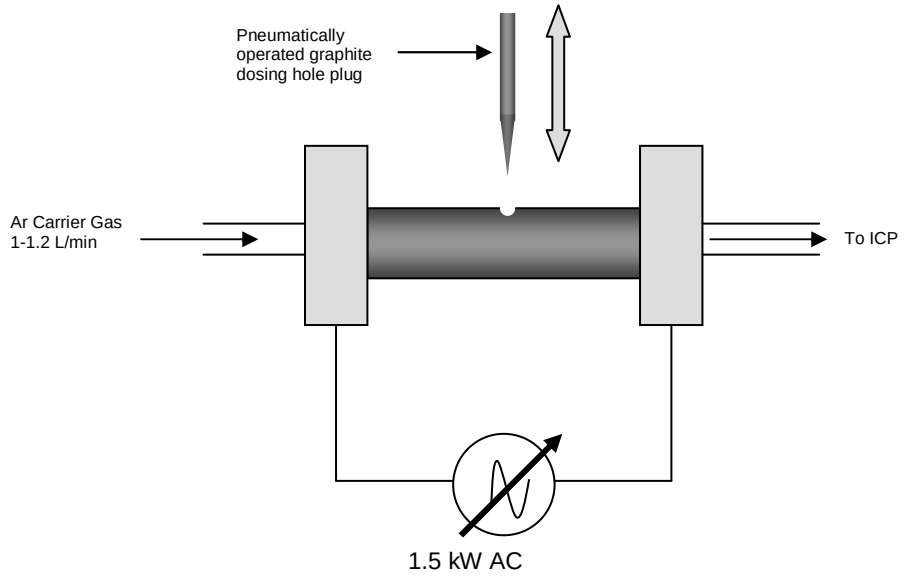

Figure 1.4: Schematic diagram of "end streaming" design for a furnace-type ETV

The sample is injected into the furnace via the small (*ca.* 3mm) dosing hole at the top of the furnace. During drying or pyrolysis steps (see ETV heating program in Figure 1.5 below), the dosing hole is open and a flow of Ar (*ca.* 1 L/min) vents most solvent vapors out of the furnace. This prevents the copious amount of solvent vapor from being sent to the ICP which can cause plasma quenching. When the furnace is ready to send the sample to the ICP, the dosing hole plug *(e.g.*, a graphite rod) seals the furnace and the gas flow carries the furnace contents to the ICP.

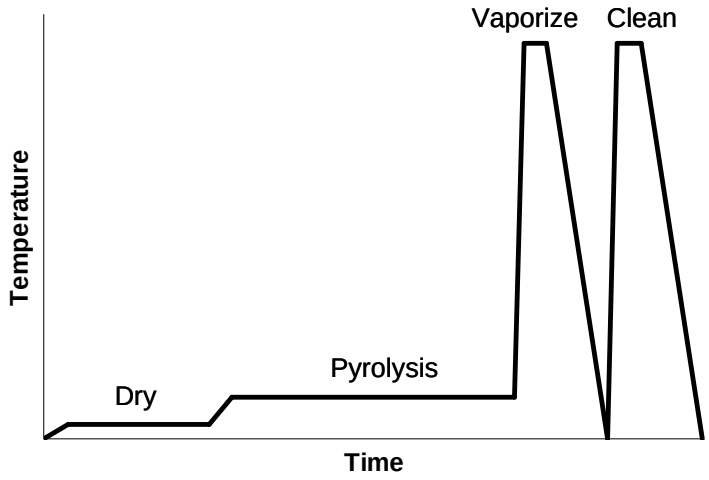

Figure 1.5: A typical heating for a graphite tube-type ETV

For aqueous samples, a dry, pyrolysis, vaporize and clean step are used. When driving off the majority of the solvent in the dry step, the temperature ramp is sufficiently slow (*ca.* 20 ˚C/sec) from room temperature to ca. 80 ˚C to prevent the sample from rapidly boiling, which will decrease precision and held for ca. 15 s. The pyrolysis step is a slow ramp to a moderate temperature (*ca.* 10 ˚C/s from 80 ˚C to 300 ˚C) to remove adsorbed water and is held for ca. 30-60 s. A fast ramp (*ca.* 1,000-2,000˚C/s) is used to vaporize the sample and is held a maximum of ~2,800 ˚C for ~5 s. The furnace is allowed to cool as rapidly as possible (*ca.* 200 ˚C/sec) before being pulsed heated back to 2,800 ˚C to clean the furnace. The clean step reduces the amount of carry over between samples.

While higher temperatures are possible in most commercially made graphite tube furnaces, the higher temperatures cause more significant carbon sublimation. The quantity of sublimated carbon can be significant enough to alter the character of the

plasma and introduce changes in ionization efficiencies and ultimately analytical accuracy. The loss of C from the furnace also reduced furnace lifetime.

Pyrolitically coated graphite furnaces are generally used during to increase reproducibility[22]. The 50-100 μm thick pryolytic coating presents a less porous surface to the sample, which prevents samples from diffusing into the more porous electrographite that makes up the bulk of the furnace mass. The diffusion into the electrographite not only broadens peaks because of the need to diffuse back to the surface, the high density of active sites on the electrographite can prevent some metals from vaporizing completely and lead to "carry over" or "memory effects".

1.2.2 Advantages to ETV Sample Introduction

The advantages of the ETV are: the small, discrete sample size (~0-50μL), compatibility with complex matrix (*e.g.* high salt and biological material) and sampling non-aqueous solutions (*e.g.* organic solvents, solids, slurries and colloids). These samples can be directly introduced into the furnace with minimal sample preparation. The furnace produces a short (1-3 sec) pulse of dry aerosol particles. The particles are sufficiently small to not settle even after 3 min in a stop-flow condition[23]. The small particles remove the need for washout, equilibration or other delays that are required for nebulization [23]. The transport efficiency of the aerosol can range from as low as 3%[24] to as high as 80%[25], which is greater than the 1-5% for pneumatic nebulization with a spray chamber[7].

Since the vaporization or desorption of the analytes are dependent on the furnace temperature, the transient nature ETV generated pulse permits some separation of species with respect to their arrival time at the ICP and ultimately the MS detection system. Thus, some isobaric interferences can be minimized based on the differences in their evolution times from the ETV. While the generation function in the ETV can be quite sharp,

broadening of this pulse as a consequence of laminar flow broadening during movement down the transport tube[26, 27] can be detrimental to situations where separation is desirable. Previous work has shown that proper design of the transport system can minimize this broadening (*e.g.,* use of 1.5mm instead of 6.0 mm diameter transport tubing[26, 27]. Ertas and Holcombe recently presented a relatively comprehensive look at sources of peak broadening for ETV introductions and conditions that can maximize resolution between analytes evolved at different temperatures in the ETV[26].

The removal of the matrix can aid in the reduction of spectral and possibly plasma-induced interferences. As an example, from aqueous samples, the removal of water greatly reduced the amount of $^{56}ArO^{+}$, a polyatomic interferent for $^{56}Fe^{+}$, since the major contributor of oxygen is the dissociation of water[28]. The same can be done for $^{75}As^{+}$ which can have a significant isobaric interference from $^{75}ArCl^{+}$ when chloride is present in the sample. Unlike Fe, As only has one isotope, which makes the removal or attenuation of $^{75}ArCl^{+}$ signal mandatory for low level detection of $^{75}As^{+}$.

ETVs can provide analytical simplicity to samples that would normally have to be completely dissolved before use with a more conventional nebulizer. This includes analyzing solids directly and extends to samples that are difficulty to digest of cannot afford to be diluted because of the low analyte levels (*e.g.,* fluorinated polymers[29], silicate geological materials[30], motor oils[31] or blood[32, 33]).

One of the more useful means of removing combustible matrices, including biological matrices, is the introduction of oxygen during the heating program[34]. It was first used by Kundu and Prévot and more completely explained[35-37] and exploited for biological samples[32]in applications with ETAAS. It has also found success using an ETV with ICPMS[38]. Oxygen can be introduced to the furnace when at a moderate

temperature (*ca.* 800 ˚C) to remove any carbon-containing material while leaving the metals behind for analysis[38, 39]

1.3 SCOPE OF CURRENT RESEARCH

1.3.1 Optimization of Dry Plasmas

ICPMS has a myriad of adjustable parameters (*e.g.*, gas flows, torch position, electrostatic lenses, mass analyzer) that require optimization. The Optimass 8000 has real-time signal displays that can show an operator the results of a change in any given setting. Thus, with a steady-state sample introduction system, tuning of these parameters can be accomplished by watching the signal response of a single m/z or multiple m/z values. Some of the adjustable parameters have a very profound effect on sensitivity or resolution, while other settings are less important. Many are interdependent of settings of other parameters which makes optimization an iterative process.

The dry aerosol generated by the ETV affects the plasma differently than the water saturated sample introduction channel from a nebulizer. The water added to the plasma during nebulization can change the plasma in a way that makes optimization settings different for the dry plasma[40]. Unfortunately, the transient nature of the ETV makes tuning a tedious and time consuming task if one were to attempt optimization of the parameters using the ETV.

All ICPMS instruments have many parameters that must be optimized, and the Optimass 8000, in particular, has 21 parameters that one would like to evaluate during the tuning process. As a consequence, simple methods of optimization are often sought. The least complicated approach is to use one mass and vary the setting until the largest signal is produced, which is the method recommended for many instruments, including the Optimass[12].

Previous work that has attempted to devise ways to tune a dry plasma includes the use of Fe introduced as a metal carbonyl [40]; Ar_2 from the plasma gas [41]; Mo and Re from the resistive heating of wire filaments, [42]; Mn from a Nafion® membrane desolvated aerosol.[43], and steady state ETV heating of bulk amounts of Ag[44]. In all cases, a single *m/z* was monitored and in one case, extensive overhauling of an ETV was needed after use[44]. A steady state, dry aerosol optimization source for the ICPMS will be presented in Chapter 2. The comparison of performance using the settings derived from wet plasma optimization using a nebulizer with that using the dry optimization will be discussed.

1.3.2 The Coupling of a Pneumatic Nebulizer and ETV for Quantification of Common Isobaric Inferences

Many of the interferences found in ICPMS are polyatomic species formed from the matrix components of the sample[45]. The use of Dynamic Reaction Cells™ (DRC™)[46-48] and collision cells[48-50] have been employed in recent years to remove these interferences. In either cell, an quadrapole, hexapole or octapole[51] is used to focus the ions streaming from the ICP source and discriminate against certain side products[51, 52]. The chamber contains either an inert gas (collision cell) or a reactive gas (DRC™). The reactive gas in a DRC™ is often NH_3[46, 53], but CH_3[53-59], CO[53], O_2,[53, 54, 56] NO[56], H_2[56] or mixtures of reaction gasses[60]. The reactive gas produces gas phase reactions that either remove an interferent or reacts with the desired analyte to move it to a interference-free mass region[51].

Thermal pre-treat steps in the ETV can be used to remove many of the matrix components to form a matrix-free, transient signal. An ETV can be adapted to work with any instrument that is available, unlike a collision cell or DRC™. Common matrix components (Cl^-, H_2O, C) can produce polyatomic isobars ($^{40}Ar^{35}Cl^+$, $^{40}Ar^{16}O^+$, $^{40}Ar^{12}C^+$)

that can interfere with elements of interest ($^{56}Fe^{+}$[61], $^{75}As^{+}$[16, 61, 62], $^{52}Cr^{+}$[63]). Spectral overlap can occur among elements (*e.g.*, $^{116}Cd^{+}$ and $^{116}Sn^{+}$) which can be separated *via* ETV[26] instead of being removed from the sample.

The steady state nebulizer does not have these options, but has other advantages. Long integration times, abundance of literature (including government testing methods[64]) and ubiquitous commercial availability makes nebulizers a popular form of sample introduction.

When choosing a sample introduction source, the choice is exclusive (*e.g.*, one method or the other, not both). In Chapter 3, the coupling of a nebulizer and ETV will be discussed. This method will allow the advantages of the ETV (determination of a few difficult elements) and of the nebulizer (ease of use for most elements) to be used on the same instrument without the need to change out equipment. While using a full size, laboratory built ETV would be impractical, the suggestion of making a small, inexpensive device is presented.

1.3.3 Increase in Sample Throughput by Multiplexed ETV-ICPMS

The use of ETV coupled with ICPMS has not seen widespread adoption, despite many advantages over the use of the ubiquitous pneumatic nebulizer. One of the common complaints is the low duty cycle of the ETV, which can be in the low single digit range. The furnace is held at the vaporization temperature for ca. 5 s and the total heating cycle is 180 s, giving a duty cycle of ca. 3%. This is in contrast to a nebulizer that has a duty cycle of 100%.

A multiplex ETV system using low power W filaments[65] was designed to combat this problem by multiplexing all of the drying, ashing, charring and vaporization processes. Many of the W filaments will be operated at the same time and this is the reason that a low power device is needed. The operation of 10 tube-type furnaces

simultaneously would be prohibitively cumbersome. The low power design allows the device to have a much smaller footprint. However, the W filaments suffered from the common problem of metal vaporizers (*e.g.* acid attack, oxidation and high background) that lead to the introduction of large amounts of W and WO into the plasma. The addition of 10% H_2[65] to the carrier gas stream helped to reduce the amount of W being released, but it was not completely stopped.

In Chapter 4 the W filaments of the multiplex ETV are replaced with carbon yarn. The aim of this was to maintain the low power requirements that the original device used, but gain the advantages of carbon vaporizers. Carbon yarn has been used as used as atom sources in the past[66-68] and displayed much of the properties that would be needed (*e.g.,* resistance to chemical attack, high melting point, purifiable). The figures of merit for the carbon yarn as a vaporizer will be presented.

REFERENCES

[1] Montaser, A., *Inductively Coupled Plasma Mass Spectrometry*. 1998, New York: Wiley-VCH. 964 pp.

[2] Niu, H. and R.S. Houk, *Langmuir probe measurements of the ion extraction process in inductively coupled plasma mass spectrometry-I. Spatially resolved determination of electron density and electron temperature.* Spectrochim. Acta, Part B, 1994. **49B**(12-14): p. 1283-303.

[3] Seiko Instruments Inc., Japan. (1994). *Inductively coupled plasma mass spectrometer*. 5334834.

[4] Tanaka, T., et al., *Electrostatically shielded water-cooled torch for inductively coupled plasma mass spectrometry.* Anal. Sci., 1991. **7**(4): p. 537-42.

[5] Houk, R.S., J.K. Schoer, and J.S. Crain, *Plasma potential measurements for inductively coupled plasma mass spectrometry with a center-tapped load coil.* J. Anal. At. Spectrom., 1987. **2**(3): p. 283-6.

[6] Gray, A.L., R.S. Houk, and J.G. Williams, *Langmuir probe potential measurements in the plasma and their correlation with mass spectral characteristics in inductively coupled plasma mass spectrometry.* J. Anal. At. Spectrom., 1987. **2**(1): p. 13-20.

[7] Montaser, A. and Editor, *Inductively Coupled Plasma Mass Spectrometry*. 1998, New York: VCH. 964 pp.

[8] Scott, R.H., et al., *Inductively coupled plasma-optical emission analytical spectrometry.* Anal. Chem., 1974. **46**(1): p. 75-80.

[9] Montaser, A., D.W. Golightly, and Editors, *Inductively Coupled Plasmas in Analytical Atomic Spectrometry*. 1987, Weinheim, Germany: VCH. 600 pp.

[10] Industrial, Scientific and Medial Equipment, 47CFR, Pt. 18.301 (2002)

[11] R.Lide, D., ed. *CRC Handbook of Chemistry and Physics, Internet Version 2005*. 2005, CRC Press: Boca Raton.

[12] GBC Scientific Equipment Ltd.., *OptiMass 8000 Inductively Coupled Plasma Orthogonal Time-of-Flight Mass Spectrometer Operation Manual*. 2004.

[13] Venable John, D., D. Langer, and A. Holcombe James, *Optimizing the multielement analysis capabilities of an ICP quadrupole mass spectrometer using electrothermal vaporization sample introduction.* Anal. Chem., 2002. **74**(15): p. 3744-53.

[14] Vanhaecke, F., et al., *Multielement Analysis of Polyethylene Using Solid Sampling Electrothermal Vaporization ICP Mass Spectrometry.* Anal. Chem., 2000. **72**(18): p. 4310-4316.

[15] Venable, J.D., D. Langer, and J.A. Holcombe, *Optimizing the Multielement Analysis Capabilities of an ICP Quadrupole Mass Spectrometer Using Electrothermal Vaporization Sample Introduction.* Anal. Chem., 2002. **74**(15): p. 3744-3753.

[16] Mahoney, P.P., et al., *Preliminary investigation of electrothermal vaporization sample introduction for inductively coupled plasma time-of-flight mass spectrometry.* Anal. Chem., 1999. **71**(7): p. 1378-83.

[17] Venable, J.D., *Fundamental studies of electrothermal vaporization as a sample introduction source for inductively coupled plasma mass spectrometry*. 2001. p. 156 pp.

[18] Gregoire, D.C. and R.E. Sturgeon, *Analyte transport efficiency with electrothermal vaporization inductively coupled plasma mass spectrometry.* Spectrochim. Acta, Part B, 1999. **54B**(5): p. 773-786.

[19] Kirkbright, G.F. and A.F. Ward, *Atomic emission spectrometry with an induction-coupled high frequency plasma source. Comparison with the inert-gas shielded premixed nitrous oxide-acetylene flame for multielement analysis.* Talanta, 1974. **21**(11): p. 1145-65.

[20] Martin-Esteban, A. and B. Slowikowski, *Electrothermal vaporization - inductively coupled plasma-mass spectrometry (ETV-ICP-MS): A valuable tool for direct multielement determination in solid samples.* Crit. Rev. Anal. Chem., 2003. **33**(1): p. 43-55.

[21] Pierson, H.O., *Handbook of Carbon, Graphite, Diamond and Fullerenes*. 1993, Park Ridge, New Jersey: Noyes Publication. 399.

[22] De Loos-Vollebregt, M.T.C. and L. De Galan, *Furnace design in electrothermal atomization-atomic absorption spectrometry.* Spectrochim. Acta, Part B, 1988. **43B**(4-5): p. 439-49.

[23] Balsanek, W.J., J.D. Venable, and J.A. Holcombe, *Generation of a square wave inductively coupled plasma scanning mass spectrometry signal using electrothermal vaporization sample introduction.* J. Anal. At. Spectrom., 2003. **18**(1): p. 59-64.

[24] Millard, D.L., H.C. Shan, and G.F. Kirkbright, *Optical emission spectrometry with an inductively coupled radiofrequency argon plasma source and sample introduction with a graphite rod electrothermal vaporization device. Part II. Matrix, inter-element and sample transport effects.* Analyst (Cambridge, U. K.), 1980. **105**(1250): p. 502-8.

[25] Ertas, G. and J.A. Holcombe, *Determination of absolute transport efficiencies of Be, Cd, In, Pb and Bi for electrothermal vaporization sample introduction into an inductively coupled plasma using an in-line electrostatic precipitator.* Spectrochim. Acta, Part B, 2003. **58B**(9): p. 1597-1612.

[26] Ertas, G. and J.A. Holcombe, *Optimization of ETV-ICP(TOF)MS and transient signal profiles for reducing isobaric interferences.* J. Anal. At. Spectrom., 2005. **20**(8): p. 687-695.

[27] Venable, J. and J.A. Holcombe, *Peak broadening from an electrothermal vaporization sample introduction source into an inductively coupled plasma.* Spectrochim. Acta, Part B, 2001. **56B**(8): p. 1431-1440.

[28] Niu, H. and R.S. Houk, *Fundamental aspects of ion extraction in inductively coupled plasma mass spectrometry.* Spectrochim. Acta, Part B, 1996. **51B**(8): p. 779-815.

[29] Resano, M., et al., *Direct multi-element analysis of a fluorocarbon polymer via solid sampling-electrothermal vaporization-inductively coupled plasma mass spectrometry.* J. Anal. At. Spectrom., 2006. **21**(9): p. 891-898.

[30] Ben Younes, M.E., D.C. Gregoire, and C.L. Chakrabarti, *Vaporization and removal of silica for the direct analysis of geological materials by slurry sampling electrothermal vaporization-inductively coupled plasma-mass spectrometry.* J. Anal. At. Spectrom., 1999. **14**(11): p. 1703-1708.

[31] Langer, D. and J.A. Holcombe, *A method for the direct analysis of new and used lubricating oils using electrothermal vaporization inductively coupled plasma mass spectrometry (ETV-ICPMS).* Prepr. - Am. Chem. Soc., Div. Pet. Chem., 1999. **44**(3): p. 274-278.

[32] Eaton, D.K. and J.A. Holcombe, *Oxygen ashing and matrix modifiers in graphite furnace atomic absorption spectrometric determination of lead in whole blood.* Anal. Chem., 1983. **55**(6): p. 946-50.

[33] Li, S., et al., *Direct determination of trace refractory elements in human serum by ETV-ICP-MS with in-situ matrix removal.* Anal. Bioanal. Chem., 2004. **379**(7-8): p. 1076-1082.

[34] Kundu, M.K. and A. Prevot, *Oxygen-rich atmosphere for direct determination of copper in oils by nonflame atomic absorption spectrometry.* Anal. Chem., 1974. **46**(11): p. 1591-5.

[35] Salmon, S.G., *Effect of oxygen on analyte vaporization and gas phase reaction in electrothermally heated graphite atomizers*. 1981. p. 260 pp.

[36] Salmon, S.G. and J.A. Holcombe, *Alteration of metal release mechanisms in graphite furnace atomizers by chemisorbed oxygen.* Anal. Chem., 1982. **54**(4): p. 630-4.

[37] Salmon, S.G., R.H. Davis, Jr., and J.A. Holcombe, *Time shifts and double peaks for lead caused by chemisorbed oxygen in electrothermally heated graphite atomizers.* Anal. Chem., 1981. **53**(2): p. 324-30.

[38] Fonseca, R.W., et al., *Effect of oxygen ashing on analyte transport efficiency using ETV-ICP-MS.* Appl. Spectrosc., 1997. **51**(12): p. 1800-1806.

[39] Miller-Ihli, N.J. and S.A. Baker, *Microhomogeneity assessments using ultrasonic slurry sampling coupled with electrothermal vaporization isotope dilution inductively coupled plasma mass spectrometry.* Spectrochim. Acta, Part B, 2001. **56B**(9): p. 1673-1686.

[40] Jakubowski, N., I. Feldmann, and D. Stuewer, *Diagnostic investigations of aerosols with varying water content in inductively coupled plasma mass spectrometry.* J. Anal. At. Spectrom., 1993. **8**(7): p. 967-77.

[41] Gray, D.J., S. Wang, and R. Brown, *Stability and sensitivity enhancement using ETV-ICPMS.* Appl. Spectrosc., 1994. **48**(11): p. 1316-20.

[42] Doherty, W., P.M. Outridge, and D.C. Gregoire, *Technique for the introduction of dry atomic vapors for improved optimization and diagnostic studies of laser ablation inductively coupled plasma spectrometry.* J. Anal. At. Spectrom., 1996. **11**(11): p. 1123-1126.

[43] Yang, J., et al., *Use of a multi-tube Nafion membrane dryer for desolvation with thermospray sample introduction to inductively coupled plasma-atomic emission spectrometry.* Spectrochim. Acta, Part B, 1996. **51B**(12): p. 1491-1503.

[44] Langer, D.L., *Electrothermal vaporization inductively coupled plasma mass spectrometry: fundamental studies and practical applications*. 2000, University of Texas - Austin. p. 149 pp.

[45] Tan, S.H. and G. Horlick, *Background spectral features in inductively coupled plasma/mass spectrometry.* Appl. Spectrosc., 1986. **40**(4): p. 445-60.

[46] Tanner, S.D and Bavanov, I.V. (1998). *Bandpass reactive collision cell*. 98-CA5369856030.

[47] Vollkopf, U., V. Baranov, and S. Tanner, *ICP-MS multielement analysis at sub-ppt levels applying new instrumental design concepts.* Spec. Publ. - R. Soc. Chem., 1999. **241**(Plasma Source Mass Spectrometry): p. 63-79.

[48] Rowan, J.T. and R.S. Houk, *Attenuation of polyatomic ion interferences in inductively coupled plasma mass spectrometry by gas-phase collisions.* Appl. Spectrosc., 1989. **43**(6): p. 976-80.

[49] Morton, J., et al., *ICP-MS applications.* Inductively Couples Plasma Mass Spectrometry Handbook, 2005: p. 385-396.

[50] (Eiden, G. C., Barinaga, C.J., Koppenall, D.W., (1999). *An apparatus for reduction of selected ion intensities in confined ion beams*. 99-US135179966536.

[51] Tanner, S.D., V.I. Baranov, and D.R. Bandura, *Reaction cells and collision cells for ICP-MS: a tutorial review.* Spectrochim. Acta, Part B, 2002. **57B**(9): p. 1361-1452.

[52] Bandura, D.R., *Collision and reaction cells. Implementation and applications.* Inductively Coupled Plasma Mass Spectrometry Handbook, 2005: p. 352-384.

[53] Chery, C.C., et al., *Optimization of ICP-dynamic reaction cell-MS as specific detector for the speciation analysis of vanadium at therapeutic levels in serum.* J. Anal. At. Spectrom., 2003. **18**(9): p. 1113-1118.

[54] Wu, M.-C., S.-J. Jiang, and T.-S. Hsi, *Determination of the ratio of calcium to phosphorus in foodstuffs by dynamic reaction cell inductively coupled plasma mass spectrometry.* Anal. Bioanal. Chem., 2003. **377**(1): p. 154-158.

[55] Nixon, D.E., et al., *Evaluation of a tunable bandpass reaction cell inductively coupled plasma mass spectrometer for the determination of selenium in serum and urine.* Spectrochim. Acta, Part B, 2003. **58B**(1): p. 97-110.

[56] Hattendorf, B. and D. Gunther, *Strategies for method development for an inductively coupled plasma mass spectrometer with bandpass reaction cell. Approaches with different reaction gases for the determination of selenium.* Spectrochim. Acta, Part B, 2003. **58B**(1): p. 1-13.

[57] Chen, K.-L. and S.-J. Jiang, *Determination of calcium, iron, and zinc in milk powder by reaction cell inductively coupled plasma mass spectrometry.* Anal. Chim. Acta, 2002. **470**(2): p. 223-228.

[58] Kumar Danadurai, K.S., Y.-L. Hsu, and S.-J. Jiang, *Determination of selenium in nickel-based alloys by flow injection hydride generation reaction cell inductively coupled plasma mass spectrometry.* J. Anal. At. Spectrom., 2002. **17**(5): p. 552-555.

[59] Sloth, J.J. and E.H. Larsen, *The application of inductively coupled plasma dynamic reaction cell mass spectrometry for measurement of selenium isotopes, isotope ratios and chromatographic detection of selenoamino acids.* J. Anal. At. Spectrom., 2000. **15**(6): p. 669-672.

[60] Wallschlaeger, D. and J. London, *Determination of inorganic selenium species in rain and sea waters by anion exchange chromatography-hydride generation-inductively-coupled plasma-dynamic reaction cell-mass spectrometry (AEC-HG-ICP-DRC-MS).* J. Anal. At. Spectrom., 2004. **19**(9): p. 1119-1127.

[61] Carey, J.M., et al., *Evaluation of a modified commercial graphite furnace for reduction of isobaric interferences in argon inductively coupled plasma mass spectrometry.* Spectrochim. Acta, Part B, 1991. **46B**(13): p. 1711-21.

[62] Byrne, J.P. and G. Chapple, *Direct determination of trace metals in seawater by electrothermal vaporization ICP-MS with Pd-HNO3 modifier.* At. Spectrosc., 1998. **19**(4): p. 116-120.

[63] Byrne, J.P., et al., *Determination of chromium by electrothermal vaporization inductively coupled plasma mass spectrometry.* Can. J. Anal. Sci. Spectrosc., 1997. **42**(4): p. 95-101.

[64] National Primary Drinking Water Regulations, 40 CFR, Pt. 141 (2002)

[65] Venable, J.D., M. Detwiler, and J.A. Holcombe, *Multiplexed electrothermal vaporization sample introduction system for inductively coupled plasma spectrometry.* Spectrochim. Acta, Part B, 2001. **56B**(9): p. 1697-1706.

[66] Montaser, A. and S.R. Crouch, *Analytical applications of the graphite braid nonflame atomizer.* Anal. Chem., 1974. **46**(12): p. 1817-20.

[67] Montaser, A., S.R. Goode, and S.R. Crouch, *Graphite braid atomizer for atomic absorption and atomic fluorescence spectrometry.* Anal. Chem., 1974. **46**(4): p. 599-601.

[68] West, T.S. and X.K. Williams, *Atomic absorption and fluorescence spectroscopy with a carbon filament atom reservoir. I. Construction and operation of atom reservoir.* Anal. Chim. Acta, 1969. **45**(1): p. 27-41

Chapter 2: Dry Analyte Introduction System for ICPMS Optimization Utilizing a Dry Plasma

2.1 INTRODUCTION

A steady-state signal facilitates the optimization of critical settings in an ICPMS. The nebulizer is usually the method of choice for optimization because of its steady state signal, relative ease of use and ubiquitous coupling with the ICPMS. However, it has been shown that water in the central channel does have a large impact on how the plasma behaves.[1] Consequently, for those techniques where a dry plasma is employed in analysis (*e.g.*, electrothermal vaporization, ETV, laser ablation, LA, etc.), "tuning" with a nebulizer and a water saturated vapor in the central channel is less than optimum. Laser ablation produces a nearly steady-state signal that can be used for tuning, but ETV is characterized a low duty cycle, transient signal that can make its use in plasma and spectrometer tuning extremely tedious.

Most optimization techniques, including recommendations by the manufacturer generally utilize a single mass or very small mass range, making detection of mass biased sensitivities difficult to optimize. Introducing a dry sample that is steady-state for the purposes of plasma tuning has been explored, albeit still tuning on a single element.[1-5] (Fe introduced as a metal carbonyl [1]; Ar_2 from the plasma gas [2]; Mo and Re from the resistive heating of wire filaments, [4]; Mn from a Nafion® membrane desolvated aerosol.[3], and heated bulk Ag [5]) While these were useful, a wider range of masses and physical characteristics (*e.g.*, ionization potential, volatility) should permit better selection of optimized settings.

This paper explores a steady-state, dry sample introduction system employing several elements representing a range of masses and ionization potentials. This broader tuning base will be particularly useful where the dry sample introduction source is transient in character and not easily amenable to "tuning" the plasma and optics. Our particular interest is in optimization for ETV introduction. A comparison of ETV-ICPMS performance using dry plasma optimization and wet plasma (*e.g.,* nebulizer introduction) will also be investigated.

2.2 EXPERIMENTAL

2.2.1 Reagents

All chemicals were of reagent grade or higher purity: NbF_5 (98%, Aldrich), $SnBr_4$ (99%, Aldrich), silica gel desiccant (Reagent ACS 10-18 mesh, Fisher Scientific). Industrial purity Ar was used for the plasma and carrier gases (Praxair Inc, Austin, TX). A 10 ppb 30-element multi metal solution containing Li, Be, Na, Mg, Al, K, Ca, V, Cr, Mn, Fe, Ni, Co, Cu, Zn, Ga, Ge, As, Se, Rb, Sr, Ag, Cd, In, Cs, Ba, Tl, Pb, Bi, and U was made from dilution of 10 ppm standard (PlasmaCAL, SCP Science) with 1% HNO_3 using 70% concentrated redistilled to 99.999% purity HNO_3 (Aldrich, Milwaukee, WI). A 100 ppb tuning solution of Br, Si, W, Pb and Sn was made from dilution of 1,000 ppm standards (SCP Science) and dissolution of a stock solution of KBr (Mallinckrodt). The tungsten filament was from an FLW 24V 300W (Philips, Japan) projector light bulb with the quartz envelope removed.

2.2.2 Instrumentation

All analyses were performed on an Optimass 8000 (GBC Scientific Equipment Pty. Ltd., Australia) ICPMS system, which is an orthogonally accelerated time-of-flight (*oa*-TOF) mass spectrometer coupled with an ICP torch. Samples introduced were performed using a modified Varian GTA-95, which has been described previously.[6] The samples consisted of 10 µL aliquots of 10 ppb multi metal solution; measurements were made in quadruplicate.

an applied power of 1.2 kW without a water load on the instrument used in this study, and possibly other systems, causes a secondary discharge to form beyond the sampling cone, *i.e.*, in the last skimmer region of the ion optics for this particular system. While the exact nature of the discharge is still not understood,[7-9] a substantial current flows from the skimmer cone to ground (0.1-0.5 mA). The discharge also causes a marked decrease in the signal intensity and significant sputtering and subsequent destruction of the skimmer cone.[10] It was found that a reduction of the applied power from 1.2 kW to 0.7 kW minimizes or eliminates the discharge while maximizing the sensitivity for dry plasma conditions. [9, 10] In brief, this need for reduced power operation with dry sample introduction further supports the requirement for independent optimization in the absence of solvent.

2.3 RESULTS AND DISCUSSION

2.3.1 Procedures

Optimization of a multi-dimensional system can be performed in a myriad of ways ranging from Simplex optimization to Monte Carlo annealing. However, many

approaches, such as the two noted, would require all 21 parameters, as seen on Table 2.1, of the instrument to be entered manually, intensities measured and then a new set of 21 parameters entered and repeated until an optimized parameter set is found.

Common Settings	Value	Varied Settings	Values	
			Dry	Wet
Nebulizer flow (L/min)	1.000	Torch X (mm)	5.0	6.5
Plasma flow(L/min)	10.00	Skimmer (V)	-800	-900
Auxiliary flow(L/min)	1.000	Extractor (V)	-1,500	-1,200
Torch Y (mm)	0.3	Y Mean (V)	-80	-70
Torch Z (mm)	-0.2	Y Deflection (V)	1	-2
Z(1) Lens (V)	-700	Z Lens Mean (V)	-1,050	-1,100
Fill Bias (V)	0.60	Z Lens Deflection (V)	-26	-32
Fill Grid (V)	-8.0	Lens Body (V)	-170	-160
Pushout Plate (V)	480	Fill (V)	-39.00	-35.00
Pushout Grid (V)	-480			
Reflectron (V)	580			
Multiplier Gain (V)	3,300			

Table 2.1: Comparison of the settings found from the wet optimization using the nebulizer as the sample source and the dry optimization using the dry calibrator apparatus. The Common Settings were the same for both optimization techniques. The Varied Settings changed from the Wet to Dry optimization.

This is a very time consuming method and does not utilize the already available software that permits certain parameters to be manually scanned with continuous signal

recording. To minimize the time required for the optimization, a simple algorithm was developed that uses the existing software to provide results as quickly as the data are collected.

If multiple masses are to be used then a response algorithm, R, is needed to account for preferences such as element-dependent sensitivity, weighting for one region of the spectrum versus another, or any other objectives that the analyst may wish to emphasize. In our case, the instrument was reasonably tuned so no unique weighting was given to a particular mass region.

$$R = \sum_{m/z} I_{m/z}\, W_{m/z} \qquad (2.1)$$

where $I_{m/z}$ is the intensity of a calibrant ion at *m/z*. The weighting factor, $W_{m/z}$, was set proportional to $(I^o_{m/z})^{-1}$, where $I^o_{m/z}$ is the starting intensity. $I^o_{m/z}$ will be different for each *m/z*, since each *m/z* will start at a different intensity. Using the Optimass 8000 the equation for R was entered into the system and continuously monitored as the various parameters were changed.

It should be stressed that the response algorithm used for optimization can be structured to reflect the analyst's tuning objectives. For example, if one wished to optimize the sensitivity of the heavy elements, all masses could be used but $W_{m/z}$ for heavier masses could be made disproportionately large. Thus, small changes in the intensity of the larger m/z calibrants would show a favorable change in R even when accompanied by a similar intensity loss for the low mass ions

The voltage of the electron multiplier (*i.e.*, gain) was optimized initially to minimize mass bias[11] and was only checked at the outset of the optimization

procedure. The nebulizer gas flow was then optimized, and this value used during the dry plasma optimization.

The remaining parameters were optimized, one at a time, in the order shown in Table 1 beginning with gas flows, followed by torch position, *etc*. This order addressed factors affecting sensitivity first and peak shape last. The order of adjustments starts with the lens closest to the torch and moves toward the analyzer. This process was performed three times sequentially for dry and wet optimization techniques to compensate for interdependencies of the various parameters.

In order to compare the optimized wet and dry plasma optimizations, an enhancement factor, ε, was calculated for a number of test elements using ETV-ICPMS once optimization was complete.

$$\varepsilon_{m/z} = \frac{Dry\ \ plasma\ \ I_{m/z}}{Wet\ \ plasma\ \ I_{m/z}} \qquad (2.2)$$

By defining ε in this manner, values greater than unity indicate that the dry optimization produced a larger signal.

2.3.2 Calibrant Selection

The optimization requires a steady signal for optimization. To accomplish this, new material or materials must be used. The ideal material for the dry calibrator has many attributes that must be considered: solid, easily obtained, low toxicity and compatible with the ICPMS system. Solids were preferred since liquids would be difficult to handle and contain. Low toxicity is merely a convenience for operator safety. Compatibility with the instrument removed mercury and amalgams due to concerns of

mercury deposition on instrument surfaces and persistent release. Although vapor pressures for most solids are not in the literature, these pressures can be easily determined from thermodynamic data.[12, 13] To find useful materials, the required vapor pressure was estimated from signals obtained from a typical ETV experiment. Assuming that 1 ng of sample yielding a signal approximately 1 s in duration and a gas flow rate of 1.2 L/min (20 mL/s), the ideal gas equation yields a local partial pressure of ca. 10^{-3} Pa.

Many metal halides and a few metal oxides can produce reasonable vapor pressures at ambient temperatures, and a list of possibilities was generated and their vapor pressures determined. From a list of *ca.* 100 candidates, NbF_5, $TiBr_4$ and $SnBr_4$ were isolated and then experimentally evaluated by placing a small amount of the salt into a stainless steel column between plugs of glass wool.

NbF_5 produced no measurable signal for Nb^+ and detectable signals from F^+, SiF^+ and Si^+ were seen in the mass spectrum. $TiBr_4$ yielded no detectable Ti^+ signal although Br^+ was quite pronounced. This may be the result of hydrolysis of $TiBr_4$ by trace water in the system and the subsequent formation of low volatility TiO_2 and release of HBr. $SnBr_4$ produced large signals for all the isotopes of both Sn^+ and Br^+.

Thus, elemental ions with *m/z* in the areas of 19 (F^+), 80 (Br^+) and 118 (Sn^+) were available. To obtain a high mass ion, low temperature heating of Pb placed on a W filament was employed. The filament was first electroplated with copper to aid in the wetting of the filament by Pb. A shard of lead (*ca.* 4 mg) was placed on the filament and heated under N_2 until the Pb melted onto the filament. In operation, the current to the filament was adjusted to give a reasonable $^{208}Pb^+$ signal. Interestingly, W^+ was also observed, probably as a result of volatile WO_2 forming in trace amounts on the filament

surface. In the end, the final ions and their respective first ionization potentials (in eV) include: F^+ (17.42), Si^+ (8.15), SiF^+, Br^+ (11.84), Sn^+ (7.34) and Pb^+ (7.42).

A schematic of the dry calibrator is illustrated in Figure 2.1.

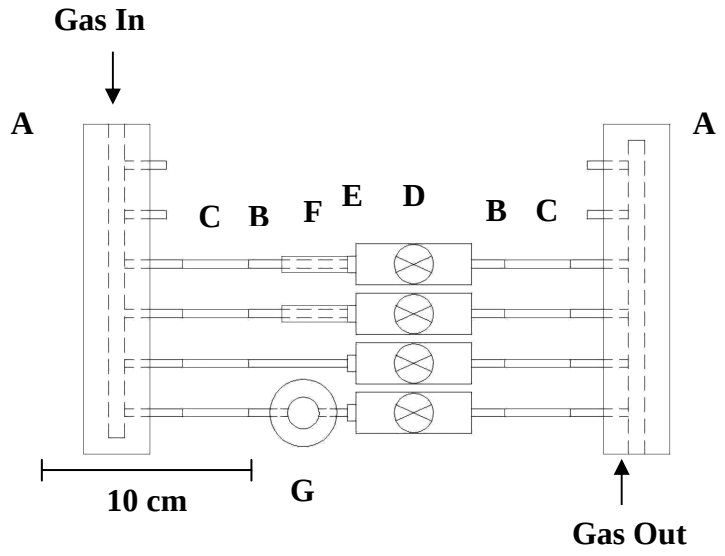

Figure 2.1: A schematic drawing of the dry calibrator apparatus is shown. Argon gas first enters a 45 cm length of ¼" Tygon® tubing that is filled with silica gel desiccant (not shown). The dry gas then enters the (A) SS Gas Manifold with 1/4" bore and 1/8" NPT outlets with a ¼" barb adaptor with ¼" NPT (not shown). The gas travels from the manifold via (B) 1/8" comp to 1/8" NPT fittings though (C) 1/8" SS tubing. The compression to NPT also connects the tubing to the (D) metering valve that controls the gas flow rate. From the metering valve the gas passes through (E) 1/8" NPT to 1/8" NPT nipple to connect to the (F) SS columns with 1/8" NPT connections. A similar arrangement is made for the adaptor for the light bulb (G) with the same array of fittings, and the holder replacing the SS column. The line without the light bulb holder or a column (second line from the bottom) is the bypass line used to provide make up gas to insure that the total flow remain constant and at the predetermined optimized value.

The halide salts were loaded into separate columns, and gas flow through each column were controlled via needle valves. The Pb signal required a balance between flow rates and filament current to achieve the desired signal. A metered bypass line (second line from the bottom in Figure 2.1) permitted adjustment of the *total* central

channel flow to a predetermined value once the flows for the individual elements were adjusted.

2.3.3 Optimization

The dry calibrator was purged of air and connected to the ICPMS to begin the process of optimization. The requirements of instrument optimization and the deviations from wet and dry plasmas will be strongly dependent on torch design, load coil geometry, applied RF frequency and applied power. For the particular instrument used in this paper and using the response function noted earlier, Table 2.1 summarizes the optimized settings using both nebulizer introduction and the dry calibrator. The first eight parameters and torch position most strongly affect the signal intensity. The remaining factors are considered to be peak shaping settings.[14] The mass resolution of the instrument is large (1,000-2,000) and fine tuning this parameter beyond the original settings was not considered in the optimization procedure.

The optimization was performed using the following algorithm:

$$R = 13 * I_{28Si} + 13 * I_{79Br} + 12 * I_{120Sn} + 10 * I_{184w} + 10 * I_{208Pb} \qquad (2.3)$$

The bias in favor of the light masses of 30% is in line with the mass bias that others have reported for time-of-flight axial accelerated ICP-TOF instruments.[15, 16] The results of the wet and dry optimization can be found on Table 2.1. As noted earlier, this algorithm is flexible and can be adjusted to the needs of a particular optimization. The behavior of $^{79}Br^{+}$ signal was similar to the other analytes, but was often more extreme. When adjusting the skimmer and extraction lens, $^{79}Br^{+}$ would increase or decrease at a faster rate than the other analytes. However, $^{79}Br^{+}$ reacted in the opposite manner as the other

analytes when adjusting the Z lens mean (*e.g.*, when the other analytes increased intensity, $^{79}Br^{+}$ decreased). The exact cause of this behavior was not apparent. Other species were available (*i.e.* $^{19}F^{+}$ and $^{47}SiF^{+}$) but were not used since three masses were already present in the low range. The $^{19}F^{+}$ and $^{47}SiF^{+}$ both behaved similarly to $^{28}Si^{+}$ in respect to changes in lens potentials. When the skimmer and extraction were adjusted, $^{19}F^{+}$ had a similar behavior to $^{79}Br^{+}$ (*e.g.*, increasing or decreasing at an exaggerated rate) including the Z lens behavior.

2.3.4 ETV Results

Once the ICPMS had been optimized, the dry calibrator was removed from the instrument and the ETV connected. The ETV will be used to evaluate the effects of dry optimization. The temperature schedule for the ETV is summarized on Table 2.2. All of the results from the ETV will be using these setting, regardless of which optimization is used on the ICP.

Temperature (℃)	Ramp (℃/sec)	Hold Time (s)	Gas (L/min)	ICP Reading?
100	15	15	1.2	
300	10	30	1.2	
300	0	15	1.000	Read
3000	1900	5	1.000	Read
50	210	0	1.000	Read
3000	2000	3	1.2	

Table 2.2: ETV settings. A 10 µL aliquot of a 10 ppb multi-element solution in 1% HNO_3 was used to determine enhancement factors.

A summery of the results of the ε. values for several elements can be seen on Figure 2.2.

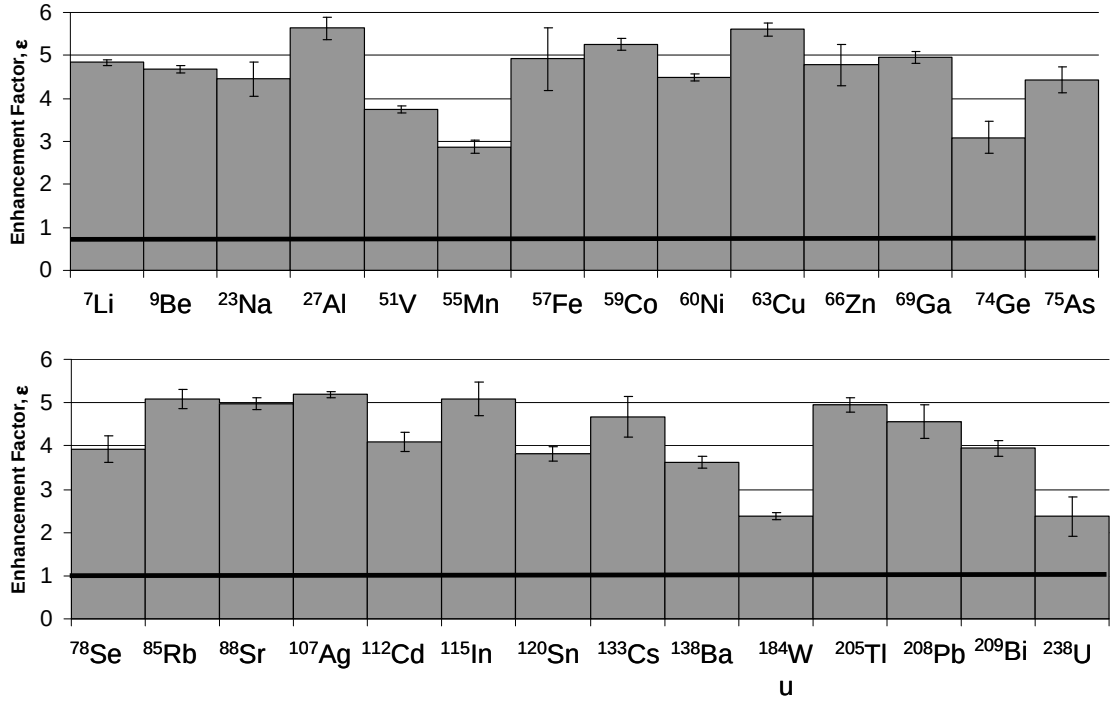

Figure 2.2: Enhancement factors (eq. 2) for several elements using ETV sample introduction. The enhancement factor ratios the signal obtained using optimized dry calibration settings to that seen using wet plasma optimization. Error bars represent ±1σ. (n=4)

The average enhancement for all of the elements shown in Figure 2.2 is 4.5±0.4; and in no instance was a loss in intensity observed as a result of using the dry calibrator to optimize the analytical conditions of the plasma or analyzer system. The Sn and W were included in the suite of elements in Figure 2.2 to demonstrate that the tuning masses were not enhanced to a greater extent than other masses. Si suffers from a significant background from $^{28}N_2$ from atmospheric gasses and the HNO_3 matrix as well as ^{28}CO. The other isotopes of Si are much less abundant (*e.g.*, ^{29}Si is ca. 5% as intense as ^{28}Si and ^{30}Si is ca. 3% as abundant), but suffer from interferences with ^{29}CO and ^{30}NO. The dry optimized parameter set was able to produce a signal that was greater than the

background. However, the wet optimized signal was indistinguishable from the background, preventing the calculation of an enhancement. Br was also monitored but failed to produce a significant signal using either parameter set. This was probably caused by the volatilization of HBr during the 300 ˚C char step and subsequently swept out of the furnace before data collection had begun. The nearly element independent enhancement indicates that the dry optimization served to better sample the plasma and focus the resulting ion stream in the ion optics region. This can be a result of the physical changes in the plasma (*e.g.* plasma pulling back into the torch) at lower applied powers and no solvent load. By sampling the plasma more efficiently, this enhanced all of the ions, but was not selective for specific properties (*i.e.* mass or ionization potential).

2.4 CONCLUSION

The differences between wet and dry plasmas are numerous (*e.g.*, lack of water and lack of oxygen). These differences are further obfuscated by the requirement to use a reduced applied power for the dry plasma operation, which adds another variable. These differences require an optimization technique that mirrors these unique conditions. The use of a dry optimization method that is compatible with the dry plasma condition when using an ETV has been shown.

The skimmer voltage and the torch's axial position (X-position) were the most important parameters when changing from the wet to dry plasma. Changing the X-position from 6.5mm to 5.0mm alone yielded an average enhancement of 1.65. Using the dry optimized value of -1,500V for the extraction voltage instead of the -1,200V from the wet optimization produced an average enhancement of 1.61. The plasma pulls back into

the torch when the applied power is reduced, which explains the enhancement from moving the torch closer to the skimmer cone. The extraction lens is one of the first lenses in the lens stack, and is thus the closest to the plasma.

While the calibrator discussed in this paper used an array of materials to achieve a range of optimization masses, a simpler device could be constructed. The device would only need $SnBr_4$ between plugs of glass wool in a piece of ¼" Tygon®, a valve to control the gas flow to the $SnBr_4$ and a bypass line would give two dry optimization masses. This simple device could be easily fabricated with minimal tools at a minimal price.

An algorithm was developed to aid the optimization. The algorithm that was used is a suggestion, and can be modified to fit the needs of a particular analysis or tailored to counter the anomalies of a particular instrument. For this study, a general purpose, low mass bias optimization was achieved. The range of elements, while finite, does represent a range of masses and ionization potentials. This did accomplish the goal of relatively flat enhancement across the mass range, indicating that mass bias was not introduced with the dry optimization technique. The variety of elements studied were shown to be useful for tuning with a dry plasma, preventing mass bias, low toxicity, and increased the average intensity.

2.5 ACKNOWLEDGEMENTS

The authors would like to acknowledge the support of National Science Foundation (CHE-0315336)) and the useful suggestions provided by Dr. Gulay Ertas.

REFERENCES

[1] Jakubowski, N., I. Feldmann, and D. Stuewer, *Diagnostic investigations of aerosols with varying water content in inductively coupled plasma mass spectrometry.* J. Anal. At. Spectrom., 1993. **8**(7): p. 967-77.

[2] Gray, D.J., S. Wang, and R. Brown, *Stability and sensitivity enhancement using ETV-ICPMS.* Appl. Spectrosc., 1994. **48**(11): p. 1316-20.

[3] Yang, J., et al., *Use of a multi-tube Nafion membrane dryer for desolvation with thermospray sample introduction to inductively coupled plasma-atomic emission spectrometry.* Spectrochim. Acta, Part B, 1996. **51B**(12): p. 1491-1503.

[4] Doherty, W., P.M. Outridge, and D.C. Gregoire, *Technique for the introduction of dry atomic vapors for improved optimization and diagnostic studies of laser ablation inductively coupled plasma spectrometry.* J. Anal. At. Spectrom., 1996. **11**(11): p. 1123-1126.

[5] Langer, D.L., *Electrothermal vaporization inductively coupled plasma mass spectrometry: fundamental studies and practical applications*. 2000, University of Texas - Austin. p. 149 pp.

[6] Langer, D. and J.A. Holcombe, *Thermophoretic Collection and Analysis of Submicrometer Ag Particles Emitted from a Graphite Tube-Type Electrothermal Vaporizer.* Anal. Chem., 1999. **71**(3): p. 582-588.

[7] Sakata, K., N. Yamada, and N. Sugiyama, *Ion trajectory simulation of inductively coupled plasma mass spectrometry based on plasma-interface behavior*. Spectrochim. Acta, Part B, 2001. **56B**(7): p. 1249-1261.

[8] Niu, H. and R.S. Houk, *Fundamental aspects of ion extraction in inductively coupled plasma mass spectrometry.* Spectrochim. Acta, Part B, 1996. **51B**(8): p. 779-815.

[9] Balsanek, W.J., *Conducting Multi-Elemental Analysis with an Inductively Coupled Plasma Mass Spectrometer Using Electrothermal Vaporization Sample Introduction*. 2005, University of Texas - Austin. p. 125 pp.

[10] Kozlov, B., A. Saint, and A. Skroce, *Elemental fractionation in the formation of particulates, as observed by simultaneous isotopes measurement using laser ablation ICP-oa-TOFMS.* J. Anal. At. Spectrom., 2003. **18**(9): p. 1069-1075.

[11] Tian, X., et al., *Accuracy and precision of lead isotope ratios in wines measured by axial inductively coupled plasma time of flight mass spectrometry.* J. Anal. At. Spectrom., 2000. **15**(7): p. 829-835.

[12] R.Lide, D., ed. *CRC Handbook of Chemistry and Physics, Internet Version 2005*. 2005, CRC Press: Boca Raton.

[13] Chase, M.W., Jr., et al., *JANAF thermochemical tables, 1982 supplement.* J. Phys. Chem. Ref. Data, 1982. **11**(3): p. 695-940.

[14] Sturgeon, R.E., J.W.H. Lam, and A. Saint, *Analytical characteristics of a commercial ICP orthogonal acceleration time-of-flight mass spectrometer (ICP-TOFMS).* J. Anal. At. Spectrom., 2000. **15**(6): p. 607-616.

[15] Emteborg, H., et al., *Isotope ratio and isotope dilution measurements using axial inductively coupled plasma time of flight mass spectrometry.* J. Anal. At. Spectrom., 2000. **15**(3): p. 239-246.
[16] Myers, D.P., et al., *Isotope ratios and abundance sensitivity obtained with an inductively coupled plasma-time-of-flight mass spectrometer.* J. Am. Soc. Mass Spectrom., 1995. **6**(10): p. 920-7.

Chapter 3: Simultaneous ETV and Nebulizer Sample Introduction System for ICPMS

3.1. INTRODUCTION

Polyatomic interferences are a constant problem in ICPMS[1], *e.g.,* $^{51}V^{+}$, $^{56}Fe^{+}$, $^{75}As^{+}$ and $^{80}Se^{+}$. Collision cells have had a major effect on reducing these interferences, and several publications report on the selection and use of various gasses, *e.g.*, NH_3[2, 3], CH_4[3-9], CO[3], O_2[3, 4, 6], NO[6], H_2[6] or mixtures of reaction gasses[10]. The gas phase reaction can remove an interference or move the analyte to a interference-free region of the spectra[11]. While available on some instruments, the addition of a collision cell to an existing instrument is not a practical option. Mathematical correction algorithms are more straightforward and are often included in the ICPMS instrument software to remove elemental isobar interferences.

The addition of ancillary gasses to the central channel is another technique for the reduction of certain interferences[12, 13]. The addition of H_2, N_2, He or Xe to the central channel has also been suggested as a means of decreasing matrix effects[12], although there is still some debate[14]. In some instances the added molecular gas serves an alternate function. For example, the addition of O_2 to the central gas was to prevent the deposition of C onto the skimmer cone. However, this did not necessarily increase the signal intensities.[12]. In all of these cases, the analyte was delivered *via* conventional solution pneumatic nebulization.

Some of the benefits of a collision cell and/or alternate gases can be realized by using an electrothermal vaporizer (ETV) sample introduction source. For example, an ETV has been shown to remove matrix components such as H_2O and Cl, which can lead to interferences with $^{56}Fe^{+}$[15] and $^{75}As^{+}$[15-17] through the formation of $^{75}ArCl^{+}$ and

$^{56}ArO^{+}$. Significant amounts of water and Cl are removed in the dry or char stage of the furnace heating cycle. This should also aid in the removal of $^{51}ClO^{+}$, which was cited as the species responsible for isobaric interference with $^{51}V^{+}$. Without H_2O and Cl present, the background at *m/z* 56 and 75 is significantly reduced, which leads to improved detection limits for these elements[1, 18].

An alternative approach is to remove the matrix before it is sent to the plasma. The short pulse from the ETV creates a signal that has a very high signal-to-background ratio and has been used to differentiate argide isobars such as $^{75}ArCl$, ^{56}ArO and ^{52}ArC from the elemental isobars for $^{56}Fe^{+}$[15], $^{75}As^{+}$[15-17] and $^{52}Cr^{+}$[19], respectively. Spectral overlap can also occur among elements (*e.g.,* $^{116}Cd^{+}$ and $^{116}Sn^{+}$, $^{87}Rb^{+}$ and $^{87}Sr^{+}$, $^{113}Cd^{+}$ and $^{113}In^{+}$, *etc*.) which can be thermally separated *via* ETV without external separation to isolate the interfering isobars. [17, 20]

Usually, analyses are performed exclusively with either a nebulizer or an ETV, which removes the benefit of one of the techniques. Switching from the nebulizer to the ETV generally requires the addition of valves[18] and tubing, which is not a trivial task, often requiring the instrument to be shut down and restarted. This study examines a relatively simple configuration that permits the addition of an ETV as a supplement to nebulization.

3.2. EXPERIMENTAL

3.2.1 Reagents

All chemicals were of reagent grade or higher purity. Industrial purity Ar was used for the plasma and carrier gases (Airgas Inc, Austin, TX). All glassware was soaked in 4M HNO_3 overnight before use and rinsed with deionized, distilled water. A 10 ng/L 30-element multimetal solution containing Li, Be, Na, Mg, Al, K, Ca, V, Cr, Mn, Fe, Ni,

Co, Cu, Zn, Ga, Ge, As, Se, Rb, Sr, Ag, Cd, In, Cs, Ba, Tl, Pb, Bi, and U was made by dilution of 10 μg/L standard (PlasmaCAL, SCP Science) with 1% HNO_3 using 70% concentrated redistilled to 99.999% purity HNO_3 (Aldrich, Milwaukee, WI) or 1% HCl made from Trace Metal Grade HCl (Fisher Scientific, Pittsburg, Pa).

3.2.2 Instrumentation

A GBC Optimass 8000 (GBC Scientific Equipment Pty. Ltd., Australia) ICP(TOF)MS was used for all analyses. A modified Varian GTA-95 electrothermal vaporizer, which has been previously described [21], was used for comparison studies. A cyclonic spray chamber (Glass Expansion, Melbourne, Australia) and concentric glass nebulizer (C type, Precision Glassblowing, Centennial, CO) were used for all nebulizer based studies.

3.2.3 Coupling an ETV with a Nebulizer

The transient pulse of the ETV allows the detection of elements from argide isobars. The signal from the ETV should appear as a peak above the steady state background from the nebulizer signal. In order to gain the benefits from a nebulizer and an ETV, a method of combining the two techniques to work simultaneously was devised. While some spray chambers have auxiliary input ports, it was necessary to insert a glass T at the exit of the spray chamber as shown in Figure 3.1.

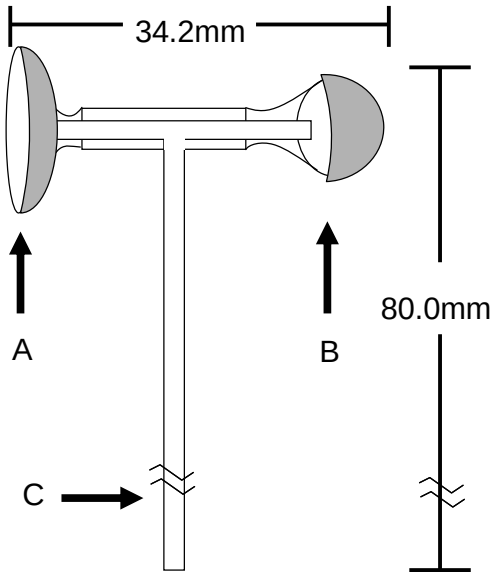

Figure 3.1: The 12/5 Socket (A) of the glass T connects to the ball join on the end of the GBC torch; the spray chamber attaches to the 12/5 Ball Joint (B). 4mm i.d tubing (C) is used to connect the ETV tubing supplying the central gas channel of the torch.

Since the Optimass requires a gas flow in the central channel to prevent a secondary discharge in the skimmer cone region [22], two valves were used to maintain the central gas flow[18]. The gas routing is illustrated in Figure 3.2 and shows the placement of the glass T in relation to the spray chamber, torch and ETV. It should be noted that minimal sample is lost in the valve, probably as a result of the aerodynamically small size of the aerosol particles[21].

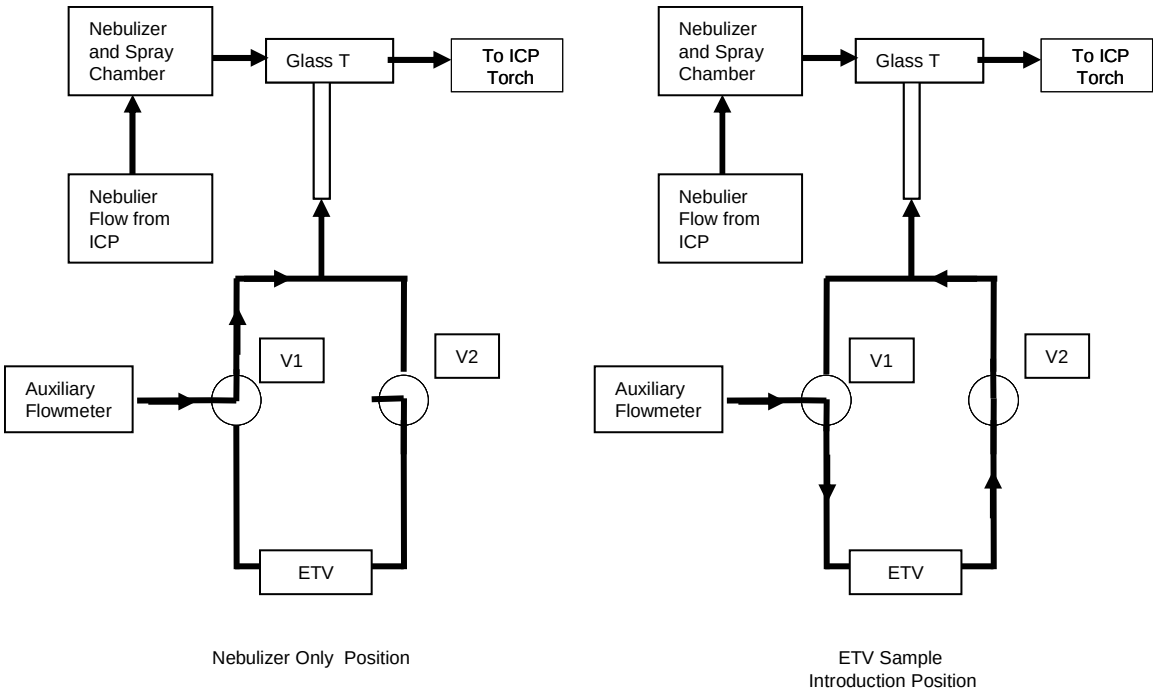

Figure 3.2: Gas routing diagram used with the glass T. The 'Nebulizer Only Position" is used when only the nebulizer introduction is used. This includes the periods when the ETV is loading and in the drying stages. The " ETV Sample Introduction Position" is used when the ETV is vaporizing a sample for introduction into the torch.

3.2.4 Dry Plasma with the GBC Optimass 8000

The small, dry particles from the ETV act differently in the plasma than the small droplet of solution from the nebulizer. It is well known that instrument settings and torch position can vary significantly depending on the introduction of a wet or dry aerosol into the ICP. For optimal operation, the instrument required *ca.* 1 L/min of Ar in the central channel. Normally, 100% of this would have sent to the nebulizer to facilitate nebulization or to the ETV to sweep material out of the furnace. With the combination of the two, the gas has to be split between the two sources, giving neither source the optimal gas flow. Previously, it has been shown that the Optimass must be operated at a reduced applied power when utilizing a dry plasma with laser ablation [22] and ETV[14].

However, the presence of water vapor in the central channel is the only requisite if the instrument is to operate successfully at 1.2 kW, which is the optimal applied power for pneumatic nebulization. Therefore, to operate the instrument at 1.2 kW with the ETV, water must be introduced to the plasma simultaneously. With a reduced gas flow to the nebulizer (*i.e.*, 0.2 L/min instead of 1.0 L/min), it was expected that nebulization efficiency would be low, but still contributing some water. Not surprisingly, aspiration of 1% HCl even at 0.2 L/min yields a significant $ArCl^+$ signal at *m/z* 75 as well as the ArO^+ signal characteristic of water introduction into the plasma.

3.3 RESULTS AND DISSCUTION

The coupling of the ETV and nebulizer was intended to harness the advantages of the ETV as a *supplement*, not replacement, for the nebulizer. This means that the performance of the nebulizer should not be compromised. This condition may result in the performance of the ETV being less than would be expected as a stand alone system. This would entail using the nebulizer optimized setting for the instrument, which is shown in Table 3.1.

ICP Settings

	Varied Settings		
	Wet Optimized	Dry Optimized	
Nebulizer	On	On	Off
Skimmer (V)	-800	-600	-700
Extraction (V)	-1,100	-650	-1,200
Z1 (V)	-800	-700	-800
Y Mean (V)	-60	-90	-70
Y Deflection (V)	-1	-3	-2
Z Lens Mean (V)	-1,100	-960	-980
Z lens Deflection (V)	-30	-35	-30
Lens Body (V)	-157	-150	-155
Fill Grid (V)	-20	-20	-20
Pushout Grid (V)	-540	-510	-510
Muliplier Gain (V)	3,450	2,200	2,200
X position (mm)	11	16	16
Z position (mm)	0.1	0.4	0.4
ICP Neb gas (L/min)	0.20	0.20	0.00
Aux. Flowmeter (L/min)	0.80	1.15	1.45

Common Settings	
Plasma Flow (L/min)	10.3
Aux Flow (L/min)	1.1
Applied Power (W)	1,200
Reflectron (V)	580
Pushout Plate (V)	510
Y Position (mm)	1.6
Pump (RPM)	5
Fill (V)	-33
Fill Bias (V)	-0.3

ETV Setings

Temperature (℃)	Ramp (℃/sec)	Hold Time (s)	Gas (L /min)	ICP Reading?
100	15	15	1.2	
300	10	30	1.2	
300	0	15	Aux. Flowmeter	Read
2,800	2,000	5	Aux. Flowmeter	Read
50	210	0	Aux. Flowmeter	Read
2,800	2,000	3	1.2	

Table 3.1: The settings used for both the ICPMS and the ETV are shown. Many of the ICP settings remained the same through the different optimization and are listed separately. For the Dry Optimized settings, samples were run with the nebulizer "on" (*e.g*, flowing sample and gas) and with the nebulizer "off" (*e.g*, no sample or gas through the nebulizer). The ETV settings were used on all of the experiments. The gas flow rate through the furnace during vaporization is determined by the aux. flowmeter and varies by optimization.

With the Optimass 8000's software, maintaining the nebulizer optimized settings would be the only way to seamlessly couple the two devices, as switching optimizations is not an option when running an analytical method. Operating with the nebulizer-optimized settings represents an extreme that favors the use of the nebulizer. To test the full potential of the glass T, optimizations were explored to find the best performance of the ETV, representing the other extreme where ETV performance is paramount to nebulizer performance.

3.3.1 Impact of Glass T on Nebulizer Results

The effects of inserting the glass T (Figure 3.2) on the analytical results using the nebulizer were examined. The 4 mm tube was closed using a short length of Tygon® tubing and a clamp, and a 100 ppb multi metal solution was nebulized with and without the glass T in place. An enhancement factor, ε, was calculated as follows:

$$\varepsilon = \frac{\text{Signal with glass T}}{\text{Signal without glass T}} \tag{3.1}$$

As can be seen in Table 3.2, the glass T had no statistically significant impact on the 26 elements evaluated. The average ε for the elements presented is 1.00±0.02.

	Enhancement Factor (ε)		Enhancement Factor (ε)
^{7}Li	0.98	^{75}As	0.99
^{9}Be	1.01	^{78}Se	0.99
^{27}Al	1.02	^{85}Rb	1.00
^{51}V	0.99	^{88}Sr	1.00
^{53}Cr	0.99	^{107}Ag	0.99
^{55}Mn	1.00	^{114}Cd	1.00
^{56}Fe	0.99	^{115}In	1.01
^{59}Co	1.00	^{133}Cs	1.01
^{60}Ni	1.01	^{138}Ba	1.01
^{63}Cu	0.99	^{205}Tl	1.02
^{66}Zn	0.99	^{208}Pb	1.02
^{69}Ga	1.00	^{209}Bi	1.01
^{74}Ge	1.06	^{238}U	1.01

Table 3.2: Summery of the enhancement factors (ε) for the comparison of the signals fro the nebulizer with and without the glass T in place for the elements studied. The average ε was 1.00±0.02.

The main objective of this study is to determine the feasibility of harnessing the strengths of the ETV (*e.g.*, using the transient nature of the ETV pulse to separate elements from steady state interferences) without losing the benefits of the nebulizer. To test the strengths of the ETV, two multielement standards were analyzed, one in 1% HNO_3 and a second in 1% HCl. HNO_3 is used as the baseline because of low amounts of polyatomic interferences[1]. The HCl matrix was selected for its specific $^{75}ArCl^+$ interference with monoisotopic $^{75}As^+$.

3.3.2 Results from Supplemental ETV Introduction

The addition of the ETV *via* the glass T as an aid to primarily nebulizer-based determination is explored. The ETV settings are listed in Table 3.1, while the ICP settings can also be found in Table 3.1 under the "Wet Optimized, Nebulizer On" heading. The Optimass was optimized using the conventional spray chamber and nebulizer combination. After optimization, the gas flow to the nebulizer was reduced from the optimized 1.0 L/min to 0.20 L/min and the remaining 0.80 L/min was introduced *via* the 4mm side arm on the glass T (Figure 3.1). This experiment was designed to ensure the total gas flow to the torch was the same as the optimized nebulizer gas flow.

As anticipated with finite flow through the nebulizer, the ArO^+ and $ArCl^+$ species are elevated over that obtained with a dry plasma using the ETV alone. However, even with the significant signal from these argides species, elemental peaks can be detected from the ETV introduction. It should be noted that the ETV signal can be used

to validate the presence of As, which is difficult to do for this monoisotopic species in a real sample with significant Cl present.

3.3.2.1 ETV Transient Signals

The transient ETV signals for $^{56}Fe^{+}$, $^{75}As^{+}$ and $^{115}In^{+}$ are shown in Figures 3.3-3.5, respectively.

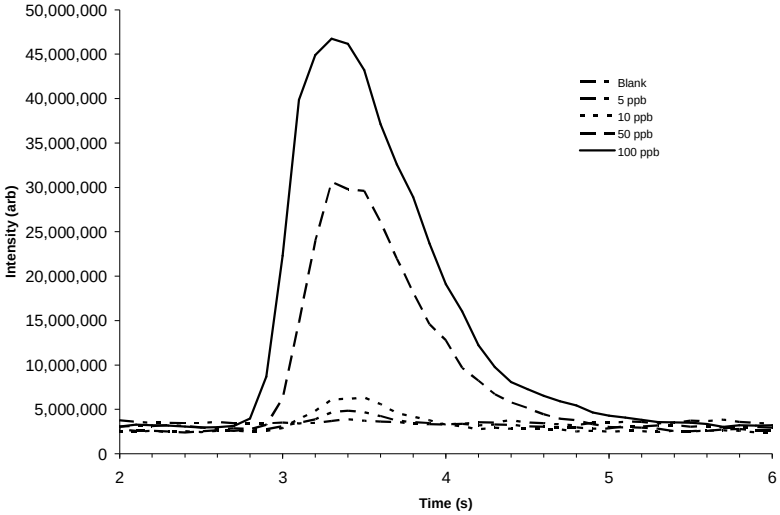

Figure 3.3: Example of $^{56}Fe^{+}$ signal from ETV vaporized sample with reduced nebulizer gas flow and nebulizer optimization

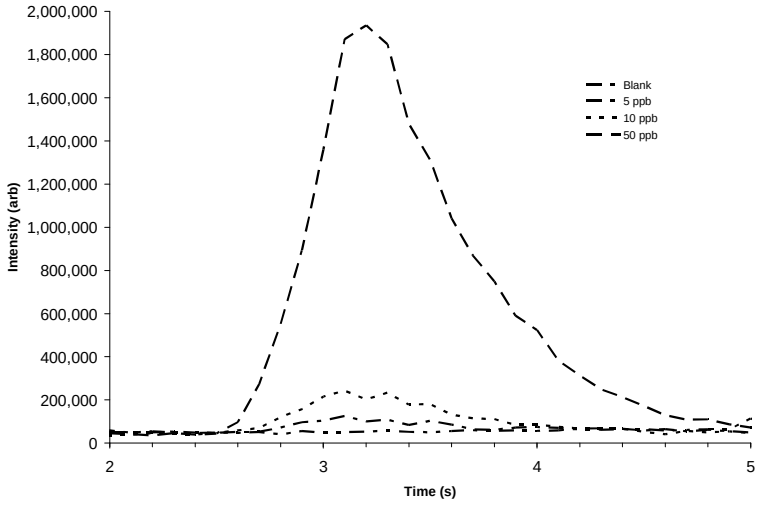

Figure 3.4: Spectra of *m/z* 75 with various amounts of $^{75}As^{+}$ added via ETV vaporization with 1% HCl aspirated with a reduced nebulizer flow rate and nebulizer optimization. The baseline is elevated due to the introduction of HCl via nebulizaition.

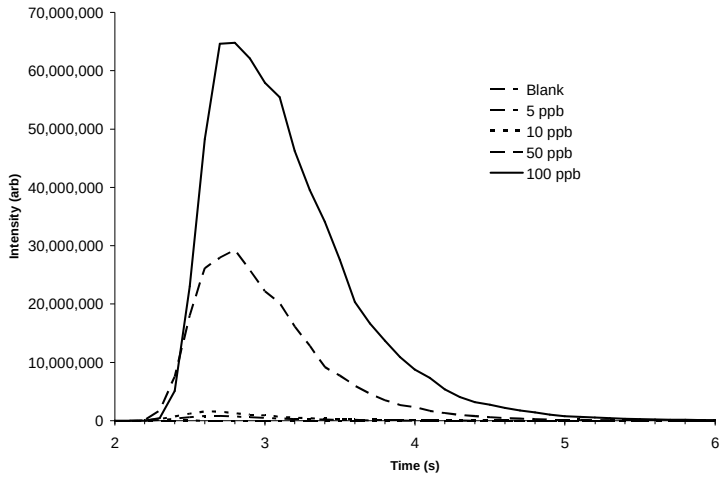

Figure 3.5: Spectrum of $^{115}In^{+}$ at various concentrations. The peaks are indicative of In introduced via the ETV vaporization with insignificant contribution of a steady state signal from the reduced gas flow nebulizer and nebulizer optimization.

Calibration curves using the ETV peak areas were linear, thus suggesting the use of the ETV-nebulizer combination as a quantitative tool as well as a simple means of validating that an element is present when an isobaric interference exists, *e.g.*, $^{75}As^{+}$ in presence of $^{75}ArCl^{+}$. The more commonly used peak areas were employed in all determinations and yielded linear calibration curves. The detection limits for several elements in the multi-element solution can be found in Table 3.3. Reference values for ETV and nebulizer can be found in Table 3.4.

A

		^{7}Li	^{27}Al	^{51}V	^{53}Cr	^{55}Mn	^{56}Fe	^{59}Co	^{63}Cu
Nebulizer Optimized	Nebulizer On	0.82	0.84	0.048	0.30	0.035	1.2	0.12	0.51
ETV Optimized	Nebulizer On	0.022	0.33	0.083	0.48	0.029	1.1	0.013	0.056
ETV Optimized	Nebulizer Off	0.042	0.63	0.007	0.15	0.19	1.0	1.7	0.04

		^{66}Zn	^{69}Ga	^{75}As	^{78}Se	^{85}Rb	^{88}Sr	^{107}Ag	^{114}Cd
Nebulizer Optimized	Nebulizer On	3.8	0.064	0.63	0.73	0.032	0.08	0.048	2.3
ETV Optimized	Nebulizer On	0.29	0.010	0.015	0.65	0.061	0.007	0.002	0.039
ETV Optimized	Nebulizer Off	0.055	0.071	0.093	1.4	0.050	0..079	0.025	0.025

		^{115}In	^{133}Cs	^{138}Ba	^{205}Tl	^{208}Pb	^{209}Bi	^{238}U
Nebulizer Optimized	Nebulizer On	0.040	0.025	2.1	0.068	1.1	0.052	0.31
ETV Optimized	Nebulizer On	0.007	0.0014	0.057	0.015	0.21	0.040	0.61
ETV Optimized	Nebulizer Off	0.020	0.026	0.25	0.022	0.025	0.0028	0.087

Table 3.3A: A comparison of the detection limits (ppb) for HNO_3 with the different optimization is shown.

B

		^{7}Li	^{27}Al	^{51}V	^{53}Cr	^{55}Mn	^{56}Fe	^{59}Co	^{63}Cu
Nebulizer Optimized	Nebulizer On	0.20	7.6	5.8	8.2	0.51	1.1	0.31	1.3
ETV Optimized	Nebulizer On	0.008	0.17	0.54	0.30	0.008	5.9	0.0052	0.49
ETV Optimized	Nebulizer Off	0.025	0.064	0.008	0.50	0.026	1.1	0.0021	0.040

		^{66}Zn	^{69}Ga	^{75}As	^{78}Se	^{85}Rb	^{88}Sr	^{107}Ag	^{114}Cd
Nebulizer Optimized	Nebulizer On	0.47	1.8	6.4	19	0.063	0.59	0.0.036	0.19
ETV Optimized	Nebulizer On	0.31	0.010	1.3	1.4	0.072	0.0047	0.0.036	0.016
ETV Optimized	Nebulizer Off	0.25	0.012	0.088	0.63	0.048	0. 0011	0.0.020	0.032

		^{115}In	^{133}Cs	^{138}Ba	^{205}Tl	^{208}Pb	^{209}Bi	^{238}U
Nebulizer Optimized	Nebulizer On	0.044	0.028	0.3	0.056	0. 054	0.15	8.2
ETV Optimized	Nebulizer On	0.011	0.0011	0.025	0.027	0. 11	0.020	0.29
ETV Optimized	Nebulizer Off	0.016	0.019	0.015	0.031	0. 41	0.009	0.13

Table 3.3B: A comparison of the detection limits (ppb) for HCl with the different optimizations is shown.

To determine the detection limits of the ETV, a 62 cm length of 3 mm tubing was added to the ETV to approximate the attenuation that occurs with the glass T. Nominally, the ETV is equipped with 6mm transport tubing. ETV-ICPMS detection limits are higher with partial nebulizer flow than those observed for the ETV operated alone. This may be a result of the non-optimal conditions for the ETV.

A

	^{7}Li	^{27}Al	^{51}V	^{53}Cr	^{55}Mn	^{56}Fe	^{59}Co	^{63}Cu
ETV	0.035	0.181	0.013	0.382	0.038	0.677	0.753	0.049
Nebulizer	0.061	0.623	0.021	0.623	0.061	5.587	0.184	0.685

	^{66}Zn	^{69}Ga	^{75}As	^{78}Se	^{85}Rb	^{88}Sr	^{107}Ag	^{114}Cd
ETV	0.108	0.038	0.016	0.075	0.040	0.038	0.003	0.106
Nebulizer	0.296	0.062	0.017	1.158	0.015	0.008	0.021	0.009

	^{115}In	^{133}Cs	^{138}Ba	^{205}Tl	^{208}Pb	^{209}Bi	^{238}U
ETV	0.010	0.004	0.027	0.003	0.034	0.003	0.261
Nebulizer	0.002	0.001	0.010	0.005	0.319	0.001	0.004

B

	^{7}Li	^{27}Al	^{51}V	^{53}Cr	^{55}Mn	^{56}Fe	^{59}Co	^{63}Cu
ETV	0.042	0.350	0.030	0.362	0.022	0.862	0.983	0.058
Nebulizer	0.117	0.684	0.593	0.668	0.063	8.452	0.062	0.762

	^{66}Zn	^{69}Ga	^{75}As	^{78}Se	^{85}Rb	^{88}Sr	^{107}Ag	^{114}Cd
ETV	0.363	0.045	0.050	0.129	0.020	0.005	0.111	0.029
Nebulizer	0.388	0.091	1.488	1.168	0.011	0.009	0.043	0.010

	^{115}In	^{133}Cs	^{138}Ba	^{205}Tl	^{208}Pb	^{209}Bi	^{238}U
ETV	0.003	0.002	0.775	0.004	0.157	0.008	0.893
Nebulizer	0.005	0.002	0.005	0.001	0.371	0.004	0.005

Table 3.4: Reference values for nebulizer and ETV with both a HNO_3 (**A**) and HCl (**B**) matrix are shown.

3.3.2.2 Specific Matrix Effects on Analyte Performance

Refractory elements ($^{27}Al^{+}$, $^{51}V^{+}$, $^{53}Cr^{+}$, $^{60}Ni^{+}$, $^{138}Ba^{+}$, $^{138}U^{+}$) showed high detection limits, especially with HCl. This could be the result of the cooling of the furnace at the end of the vaporization cycle, which pulls more vapor into the torch from

the spray chamber, and perturbs the system. In Figure 3.5, there is a visible increase in *m/z* 75 intensity at *ca.* 4 s, which correlates with the end of the heating cycle.

The low gas flow rate through the furnace lengthened the transit time though the tubing, possibly causing the refractory elements to arrive at the torch during the perturbation**.** The two elements with high ionization potentials, Zn (9.39 eV) and Cd (8.99 eV), showed improved detections limits with HCl due to the high ionization potential (IP) of Cl (13.01 eV) assisting ionization. This is similar to the way C aids ionization of high IP elements[23]. No significant signal for $^{80}Se^{+}$ was detected above the $^{80}Ar_2^{+}$ signal using ETV introduction with any of the optimizations studied. The other isotopes of Se suffered from other interference from Ar, Cl and Kr (a prevalent contaminate in liquid Ar), *e.g,* $^{77}Se^{+}$ and $^{40}Ar^{37}Cl^{+}$, $^{76}Se^{+}$ and $^{36}Ar^{40}Ar^{+}$, $^{80}Se^{+}$ and $^{40}Ar^{40}Ar^{+}$, and $^{82}Se^{+}$ and $^{82}Kr^{+}$.

3.3.3 Increased Background Uncertainty from Reduced Gas Flow to Nebulizer

The nebulizer was operated in a manner that reduced the gas flow rate through the nebulizer, but maintained the same *ca*. 1 mL/min liquid flow rate. The steady state background of the polyatomics was reduced by *ca.* 100 fold in going from 1L/min to 0.2L/min nebulizer gas flow rate. However, the RSD values for $^{56}ArO^{+}$, $^{75}ArCl^{+}$ and $^{115}In^{+}$ increased from *ca.* ±10% when using the 1L/min gas flow rate through the nebulizer to ±20-50% using the 0.2 L/min flow.

The exact cause of the increase in uncertainty at the lower gas flow rate is unknown. However, since the change in gas flow rate was the only difference, this should be a candidate for the cause of the uncertainty. The time resolved spectra did not show any peridicity, indicating that the noise is occurring at a rate faster than the 0.1s data acquisition rate. The RSD values for $^{56}ArO^{+}$, $^{75}ArCl^{+}$ and $^{115}In^{+}$ were 20%, 50% and 25%, respectively. One explanation for the decrease in precision would be inconsistent

droplet formation caused the liquid rich nebulizer. The inability of the nebulizer to aspirate the entire sample could have caused liquid to accumulate at the nozzle of the nebulizer, causing a transient, partial blockage of the nebulizer. The pressure behind the liquid would increase until the liquid was quickly ejected. This could cause a burst of small droplets to form, which would increase the liquid-gas interaction.

To account for the distribution of the uncertainties, the species must be considered for their individual properties. The high uncertainty of $^{75}ArCl^{+}$ could be caused by the gaseous transport of HCl to the torch. The gas flow would be severely decreased if the nebulizer was partialy blocked. It would also show a large increase as a burst of gas breaks the droplet free. The increased interactions between the gas and liquid phases from the high surface area small droplets would allow for more HCl to enter the gas phase. The uncertainly in $^{115}In^{+}$ can be explained in a similar manner. During the partial blockage, only large droplets are released, resulting in reduced signal intensity due to poor vaporization in the plasma. When the drop breaks free, smaller droplets are formed that are more easily vaporized in the plasma, increasing signal intensity. The relatively lower uncertainty in $^{56}ArO^{+}$ can come from considering the spray chamber saturated with water. If the spray chamber is water saturated, the amount of water reaching the plasma is always quite large. The addition of some droplets of water from the nebulizer will add to the $^{56}ArO^{+}$ signal, but be small in comparison to the water saturated gas.

3.3.4 Thermal Separation of Isobars

The use of small diameter transport tubing with the ETV has been previously shown to improve the separation of elemental isobars by their volatility differences, albeit with reduced sensitivity [20]. The 3mm tubing used in this experiment was a compromise between improved thermal separation and decreased sensitivity[20]. To further enhance temporal separation of elemental isobar, a slower ETV heating ramp of

200ºC/s replaced the more routinely used *ca.* 2,000ºC/s (Table 3.1) used in this analysis. In Figure 3.6 an example of the separation of Rb and Sr at *m/z* 87 is shown. The peaks are not baseline resolved, but it can be clearly seen that there are two peaks present. A mass resolving power of 290,000 would be required to resolve these two elemental isobars.

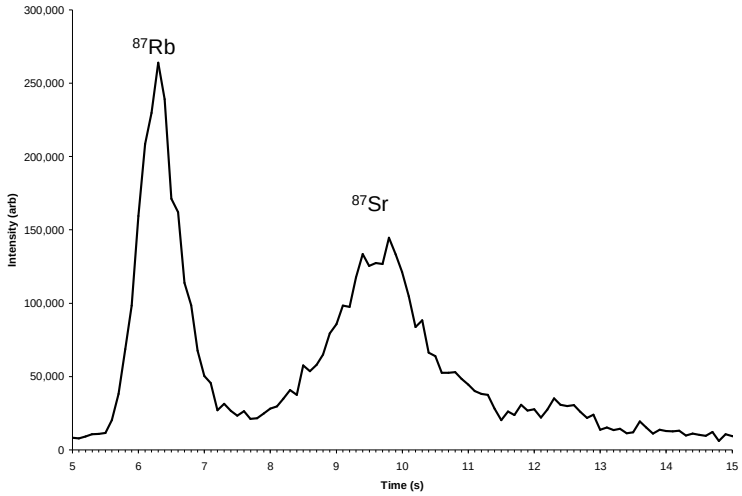

Figure 3.6: The signal from *m/z* 87 demonstrating the thermal separation of $^{87}Rb^{+}$ and $^{87}Sr^{+}$ using the glass T and the ETV with a reduced heating ramp of 250 ˚C

3.3.5 Other Optimizations

The optimization used during the previous experiments was performed to minimize the impact on solution nebulization. When compared to stand alone conventional ETV introduction, the detection limits for the glass T are higher, as shown in Tables 3.3 and 3.4. Alternate optimization techniques were explored to maximize the signal from the ETV using the glass T. It should be noted that, unfortunately, these alternate optimizations would require changes in settings that would not be possible during an analytical determination.

3.3.5.1 Dry Optimization with Wet Plasma

The first alternate optimization would replace the nebulizer as the optimization device and use an optimization source more similar to the ETV. To avoid the time consuming task of optimization using the *transient* ETV signal, the ICPMS was optimized using a continuous flow dry analyte introduction system in place of the ETV. [24] Briefly, a small amount of solid $SnBr_4$ was used as a source of dry analyte for optimization. The dry analyte was introduced into the ICPMS via the 4 mm tube on the glass T (Figure 3.2) in place of the ETV. The nebulizer and spray chamber were in place, and was permitted to nebulize with a reduced gas flow rate (0.2 L/min). A makeup gas from the auxiliary flowmeter was adjusted to maximize signal. The ICPMS was optimized utilizing $^{120}Sn^{+}$ and $^{81}Br^{+}$, and the results of the optimization can be found in Table 3.2 under the heading of "Dry Optimized, Nebulizer On."

Once the instrument was re-optimized for ETV introduction, the ETV was reconnected as shown in Figure 3.2. Detection limits were estimated using two different multimetal solutions: one in 1% HNO_3 and the other in 1% HCl. The detection limits can be found in Table 3.3, in the rows marked "ETV Optimized, Nebulizer On."

The detection limits when using the ETV optimization are improved over those using the nebulizer optimization. This is very true of the refractory elements, which are in better agreement with the detections limits that are expected from an ETV.

3.3.5.2 Dry Optimization with Dry Plasma

Since improvement of the detection limits using the dry optimization device and a wet plasma was observed, an attempt was made to optimize the ICPMS with a dry plasma. No gas or solution flowed through the nebulizer during optimization or during analysis. The same simplified dry optimization device was used to optimize the ICPMS as discussed in the previous optimization method. The results of this optimization can be

found in Table 3.1 under the category "Dry optimized, Nebulizer Off." The Optimass was operated at high applied power to mitigate any effects that water from the wet spray chamber would have on the reduced applied power (0.7 kW) plasma. The background for *m/z* 56 was elevated when compared to the ETV without the spray chamber present. The background caused by $^{56}ArO^{+}$ is reduced by *ca.* 80% and the area under the $^{56}Fe^{+}$ peak decreased by *ca.* 25% with the reduced amount of water, when compared to the ETV Optimized, Nebulizer On settings. There were no indications that a discharge occurred during analysis.

Detection limits for can be found in Table 3.3 in the "ETV Optimized, Nebulizer Off" rows. When optimized for the ETV and with no flow to the nebulizer, detection limits are generally improved.

3.4 CONCLUSIONS

Detection limits for the glass T nebulizer-ETV combination were never able to reach limits as low as those seen with stand alone ETV. This work demonstrates the basis for a device that can be used as an add-on for a nebulizer based instrument. A full graphite furnace would be impractical for this due to cost and footprint. However, any of the myriad of low power ETV devices could be suitable candidates.

3.5 ACKNOWLEDGEMENTS

The authors wish to acknowledge the support of the Nation Science Foundation (grant # CHE-0315336) and GBC Scientific Equipment. We also acknowledge the assistance of M. Ronalter for his helpful suggestions and prototype fabrications. TEK would also like to thank the Robert A. Welch Foundation for a summer fellowship.

REFERENCES:

[1] Tan, S.H. and G. Horlick, *Background spectral features in inductively coupled plasma/mass spectrometry.* Appl. Spectrosc., 1986. **40**(4): p. 445-60.

[2] Tanner, S.D and Baranov, V.I.. (1998). *Bandpass reactive collision cell*. 98-CA5369856030.
[3] Chery, C.C., et al., *Optimization of ICP-dynamic reaction cell-MS as specific detector for the speciation analysis of vanadium at therapeutic levels in serum.* J. Anal. At. Spectrom., 2003. **18**(9): p. 1113-1118.
[4] Wu, M.-C., S.-J. Jiang, and T.-S. Hsi, *Determination of the ratio of calcium to phosphorus in foodstuffs by dynamic reaction cell inductively coupled plasma mass spectrometry.* Anal. Bioanal. Chem., 2003. **377**(1): p. 154-158.
[5] Nixon, D.E., et al., *Evaluation of a tunable bandpass reaction cell inductively coupled plasma mass spectrometer for the determination of selenium in serum and urine.* Spectrochim. Acta, Part B, 2003. **58B**(1): p. 97-110.
[6] Hattendorf, B. and D. Gunther, *Strategies for method development for an inductively coupled plasma mass spectrometer with bandpass reaction cell. Approaches with different reaction gases for the determination of selenium.* Spectrochim. Acta, Part B, 2003. **58B**(1): p. 1-13.
[7] Chen, K.-L. and S.-J. Jiang, *Determination of calcium, iron, and zinc in milk powder by reaction cell inductively coupled plasma mass spectrometry.* Anal. Chim. Acta, 2002. **470**(2): p. 223-228.
[8] Kumar Danadurai, K.S., Y.-L. Hsu, and S.-J. Jiang, *Determination of selenium in nickel-based alloys by flow injection hydride generation reaction cell inductively coupled plasma mass spectrometry.* J. Anal. At. Spectrom., 2002. **17**(5): p. 552-555.
[9] Sloth, J.J. and E.H. Larsen, *The application of inductively coupled plasma dynamic reaction cell mass spectrometry for measurement of selenium isotopes, isotope ratios and chromatographic detection of selenoamino acids.* J. Anal. At. Spectrom., 2000. **15**(6): p. 669-672.
[10] Wallschlaeger, D. and J. London, *Determination of inorganic selenium species in rain and sea waters by anion exchange chromatography-hydride generation-inductively-coupled plasma-dynamic reaction cell-mass spectrometry (AEC-HG-ICP-DRC-MS).* J. Anal. At. Spectrom., 2004. **19**(9): p. 1119-1127.
[11] Tanner, S.D., V.I. Baranov, and D.R. Bandura, *Reaction cells and collision cells for ICP-MS: a tutorial review.* Spectrochim. Acta, Part B, 2002. **57B**(9): p. 1361-1452.
[12] Durrant, S.F., *Alternatives to all-argon plasmas in inductively coupled plasma mass spectrometry (ICP-MS): an overview.* Fresenius. J. Anal. Chem., 1993. **347**(10-11): p. 389-92.
[13] Montaser, A. and R.L. Van Hoven, *Mixed-gas, molecular-gas, and helium inductively coupled plasmas for analytical atomic spectrometry: a critical review.* Crit. Rev. Anal. Chem., 1987. **18**(1): p. 45-103.
[14] Balsanek, W.J., G. Ertas, and J.A. Holcombe, *The use of concomitant elements to evaluate an Ar-N2 mixed-gas plasma by electrothermal vaporization inductively coupled plasma orthogonal time-of-flight mass spectrometry.* Spectrochim. Acta, Part B, 2006. **61B**(6): p. 732-742.

[15] Carey, J.M., et al., *Evaluation of a modified commercial graphite furnace for reduction of isobaric interferences in argon inductively coupled plasma mass spectrometry.* Spectrochim. Acta, Part B, 1991. **46B**(13): p. 1711-21.
[16] Byrne, J.P. and G. Chapple, *Direct determination of trace metals in seawater by electrothermal vaporization ICP-MS with Pd-HNO3 modifier.* At. Spectrosc., 1998. **19**(4): p. 116-120.
[17] Mahoney, P.P., et al., *Preliminary investigation of electrothermal vaporization sample introduction for inductively coupled plasma time-of-flight mass spectrometry.* Anal. Chem., 1999. **71**(7): p. 1378-83.
[18] Balsanek, W.J., *Conducting Multi-Elemental Analysis with an Inductively Coupled Plasma Mass Spectrometer Using Electrothermal Vaporization Sample Introduction*. 2005, University of Texas - Austin. p. 125 pp.
[19] Byrne, J.P., et al., *Determination of chromium by electrothermal vaporization inductively coupled plasma mass spectrometry.* Can. J. Anal. Sci. Spectrosc., 1997. **42**(4): p. 95-101.
[20] Ertas, G. and J.A. Holcombe, *Optimization of ETV-ICP(TOF)MS and transient signal profiles for reducing isobaric interferences.* J. Anal. At. Spectrom., 2005. **20**(8): p. 687-695.
[21] Langer, D. and J.A. Holcombe, *Thermophoretic Collection and Analysis of Submicrometer Ag Particles Emitted from a Graphite Tube-Type Electrothermal Vaporizer.* Anal. Chem., 1999. **71**(3): p. 582-588.
[22] Kozlov, B., A. Saint, and A. Skroce, *Elemental fractionation in the formation of particulates, as observed by simultaneous isotopes measurement using laser ablation ICP-oa-TOFMS.* J. Anal. At. Spectrom., 2003. **18**(9): p. 1069-1075.
[23] Allain, P., et al., *Signal enhancement of elements due to the presence of carbon-containing compounds in inductively coupled plasma mass spectrometry.* Anal. Chem., 1991. **63**(14): p. 1497-8.
[24] Kreschollek, T. and J.A. Holcombe, *Dry analyte introduction system for ICP-MS optimization utilizing a dry plasma.* J. Anal. At. Spectrom., 2007. **22**(2): p. 171-174.

Chapter 4: Low Power, Carbon Braid Multiplexed ETV for Sample Introduction into a ICP(TOF)MS

4.1 INTRODUCTION

Atomic spectroscopists have used many different forms of electrothermal devices (*e.g.* cups, filaments, ribbons and tubes) from a variety of materials (*e.g.* W, Re, C and Ta). When used as a vaporizer for sample introduction into, for example, an ICP, the analytes need only be vaporized and not atomized, as is the case when using electrothermal atomization for atomic absorption spectrometry (ETAAS). Hence, designs that may have performed poorly for ETAAS could still be viable candidates for electrothermal vaporization (ETV).

In 1974 Kirkbright and Ward [1] were the first to show the utility of an ETV for sample introduction into an ICP. Since that time, the adoption of ETV for sample introduction has not been nearly as universal as solution nebulization. This could be due, in part, to the perception of a low sample throughput rate for the ETV. The average sample throughput for an ETV is only *ca.* 20-30 samples/h due to the thermal treatment steps before vaporization. Since the actual signal from the ETV is only *ca.* 0.5-2 s in duration, a duty cycle (*e.g.*, the ratio of temporal length of the signal and the total time to complete the analysis) of *ca.* 0.3-2% results, although the improved transport efficiency results in a 10-20 fold improvement in the instantaneous analyte delivery rate to the ICP.

Nebulizers provide a continuous signal with a duty cycle that is more difficult to calculate and dependent on the nebulizer design (*e.g.*, conventional nebulizer with spray chamber, direct injection devices, *etc.*) and how the solution flow is controlled between samples. For example, Olesik [2] suggests that spray chamber equilibration with the next sample can take several hundred seconds if acid types or concentrations vary significantly

from one sample to the next. Flow injection systems have also been used for high sample throughput (up to 150 samples/hr) using a Ryon® cross-flow nebulizer and spray chamber [3, 4], but with the caveat that large concentration changes may affect the results [3]. In such a situation, the duty cycle could be enhanced by simply lengthening the measurement period albeit at the expense of sample throughput rate. Ultimately, throughput rates can be limited in these types of devices by the equilibration times required within the sample delivery tubing or spray chambers to minimize carry over or memory effects. Since an ETV delivers a dry aerosol to the ICP with no spray chamber, such equilibration times are generally not a limiting factor.

A significantly improved sample throughput rate was demonstrated previously using a multiplexed ETV device utilizing low power, inexpensive W filaments [5]. However, the W filaments suffered from many of the problems common to metal atomizers (*e.g.*, acid attack, oxidation and high background). The addition of 10% H_2 to the Ar carrier reduced the amount of W that was sent to the plasma but did not eliminate the problem. Another limitation of the W filaments was the inability to perform oxygen ashing due to rapid oxidation of the filament.

The shortcomings of the W filament can be avoided by the use of graphite or other carbon-based materials. Graphite has the advantages of high purity, excellent chemical resistance and high operating temperatures. However, the conventional tube furnace would require unreasonable amounts of power if adapted to the multiplexed vaporizer design concept of Venable and Holcombe [5]. The requirements of a graphitic material that could replace the W filaments include a reasonably high resistance to minimize the current needed to heat the ETV, a low mass to minimize the power required, the ability to accommodate reasonable sample volumes and durability.

Graphite structures made of a solid piece of graphite lack one or more of these requirements, but carbon braids may meet the requirements.

The use of carbon braids as the thermal source for ETAAS has been previously reported [6-8]. The braids use less power ($\leq$500W) than conventional tube-type furnaces (>2 kW); while moderately successful in ETAAS, they were not competitive with the tube-type designs that are now in routine use. However, the braids in these previous studies were used as atomizers and were not evaluated as vaporizers for sample introduction into a plasma.

4.2 EXPERIMENTAL

4.2.1 Reagents

All chemicals were of reagent grade or higher purity. Industrial purity Ar was used for the plasma and carrier gases (Airgas Inc, Austin, TX). All glassware was soaked in 4M HNO_3 overnight before use and rinse with deionized, distilled water. A 10 mg/L 30-element multimetal solution containing Li, Be, Na, Mg, Al, K, Ca, V, Cr, Mn, Fe, Ni, Co, Cu, Zn, Ga, Ge, As, Se, Rb, Sr, Ag, Cd, In, Cs, Ba, Tl, Pb, Bi, and U was made by dilution of 10 μg/L standard (PlasmaCAL, SCP Science) with 1% HNO_3 using 70% concentrated redistilled to 99.999% purity HNO_3 (Aldrich, Milwaukee, WI). Bovine serum albumin (Equitech-Bio Inc., Kerrville, TX) was diluted with distilled, deionized water. The carbon braid (1.4mm dia. WYK Grade, Union Carbide) was cut into *ca.* 58 mm lengths and used as provided without any additional purification.

4.2.2 Instrumentation

A GBC Optimass 8000 (GBC Scientific Equipment Pty. Ltd., Australia) ICP(TOF)MS was used for all analyses. A modified Varian GTA-95 electrothermal vaporizer, which has been previously described [9], was used for comparison studies.

4.3 MODIFICATIONS TO MULTIPLEXED ETV

4.3.1 Overview of Modification

The basic design of the multiplexed ETV has been previously described [5]. A majority of the mechanical systems (*e.g.,* motion control, autosampler and pneumatic actuator) remained the same as in the original design. The carbon braid required the design of a system for making reproducible, low resistance contact with the filaments within the small chambers where heating would take place. Unlike the previously used W filaments, the carbon braids do not require the use of H_2, and hence the fittings and valve associated with the H_2 addition were removed, which simplified the gas handling system. The power delivery system of the original W filament equipped multiplex ETV was redesigned to handle the higher power requirements of the carbon braids (*ca.* 400 W).

4.3.2 Power Control Modification

A majority of the power control systems have been modified to meet the electrical specifications of the new carbon braid vaporizers. The original temperature control used a transistor-based feedback system to provide constant current to each filament [6]. While this design was adequate for the W filaments, the design suffered from substantial power losses in the current-controlling circuit (*i.e.,* the resistors used in the feedback

loop). The carbon braid vaporizers required more power than could be sourced from the original 24 VDC, 320 W power supply with the associated losses in the transistor-based feedback design.

The new design shown schematically in Figure 4.1 is relatively simple but is able to deliver power from any type of source (*e.g.*, AC or DC, constant voltage or constant current).

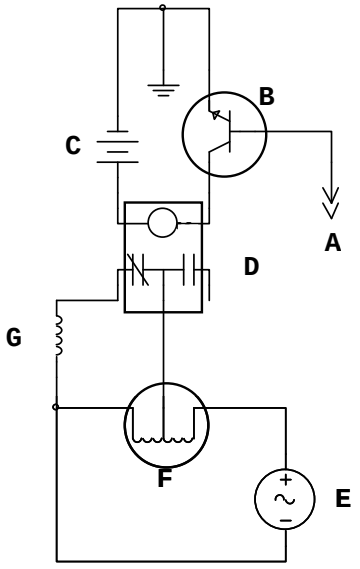

Figure 4.1: Electrical diagram of the simplified vaporization stage power supply. A 5V signal is sent from the LabView card (A) to turn on the transistor (B). The transistor allows current to pass from the 8V DC power supply (C) to circuit connected to the relay (D). Mains power (E) flows though a Variac transformer (F) to the carbon braid vaporizer (G).

The power delivery circuit used previously was a constant current source with a transistor varying the applied voltage from a constant voltage DC source. To maintain a constant current, the applied voltage needed to be changed dynamically since the resistance of the filament varies with temperature.

The LabView® program sends a 5V signal (A in Figure 4.1) to a transistor (B) that sources current from an 8V DC power supply (C) to close a relay (D). The mains (E) power a Variac® autotransformer (F) to deliver power to the carbon braid (G). The autotransformer has an output voltage range of 0 – 140VAC and could be replaced with a silicon controlled rectifier circuit similar to that commonly used with ETA supplies. The autotransformer removed the ability to adjust the temperature of the vaporization stage by software, but still permitted manual voltage adjustment.

The final temperature of the braid was measured using a disappearing filament optical pyrometer (Pyro Mico-Optical Pyrometer, The Pyrometer Instrument Co, New Jersey). The temperature measured from a disappearing filament pyrometer assumes the object is a blackbody, which is likely not the case with the carbon braid. The emissivity of different types of carbon/graphite varies from a low of 0.7 to a high of 0.9 above 2,300˚C[10]. It should be noted that emissivity changes with temperature and surface preparation as well. Even different specimens of the same material can have significant differences in emissivity. The temperature uncertainties caused by errors in estimating emissivity at the temperatures measured would be *ca*. 50˚C-90˚C[11]. The temperature of the braids measured at 32VAC and at 34VAC were 2,600˚C and 2,800˚C, respectively.

When viewed though the optical filters of the pyrometer, it was obvious that the heated braid was not a uniform temperature. Many spots were more intense than others, and even some of the filaments composing the braid were not emitting enough light to be visible. This is likely caused by poor electrical and thermal contact between the filaments composing the braid

The temperature of the Dry 1 and Dry 2 stages were measured by direct contact with a K-type thermocouple (Omega Engineering, Stamford, CT) and set to 80˚C and 220˚C, respectively. The temperature of these stages was set by adjusting the feedback circuit to achieve the desired temperature[6].

4.3.3 Braid Holders

The braid holders were designed to be compatible with the electrical connections and glass socket encasement used previously with the W filaments, which had proven to be easily sealed, rapidly flushed and compatible with the high temperature of the W vaporizer. By utilizing the same cells, it also allowed the mechanical turret to be backward compatible with W filaments. The design for the holders (Figure 4.2) consisted of a Delrin® support and Delrin® perforated disc, very similar to the ones used with the W filaments [5], as well as copper and brass electrical contacts. The braid is held in the mechanical lug (A in Figure 4.2) which provides the mechanical and electrical connections. At the end of the vaporizer's lifetime, only the braid needs to be replaced since the holders are reusable.

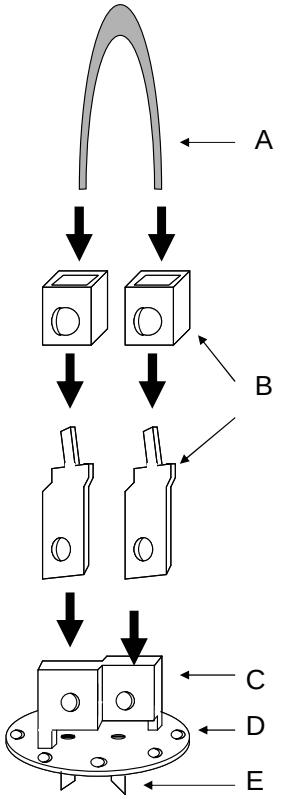

Figure 4.2: A conceptual drawing of the braid holder. The carbon braid (A) is clamped by a copper mechanical lug (B) which is screwed onto a Delrin® support (C). The support is screwed onto a Delrin® plate (D) which diffuses the sweep in the vaporize stage. Two brass pins (E) are used as the electrical connection to the socket at the bottom of the cell and are connected to the mechanical lugs (B) by a copper plate (not shown) to complete the electrical connections.

4.3.4 Gas Handling Modifications

H_2 addition to the carrier gas stream for the use of the W filaments was paramount to their success. This sort of treatment would not be needed with the carbon braid material, since the vaporized atomizer oxides (CO/CO_2) are non-condensable. In contrast, the previous filament vaporization of W as an oxide released a large amount of metal and metal oxide which disturbed the plasma and fouled sampling cones. The oxide

and accompanying degradation of the W filament was minimized using H_2 as part of the carrier gas. With the carbon-based atomizer, the H_2 gas handling equipment (*i.e.* a three-way valve and mass flow controller) was eliminated. The previous W vaporizer, multiplexed ETV was used with the Varian Ultramass, which tolerated the introduction of higher concentrations of molecular gases than the current system. Hence valves were needed to maintain an Ar flow into the central channel of the instrument at all times with the present system. Failure to maintain this central flow resulted in a secondary discharge between the second and third skimmer cones [12]. As seen in Figure 4.3, a pair of three-way valves (V1 is an Asco Model 8320G43 and V2 is a Burkert Model 0311) were used to direct the gasses to the proper lines.

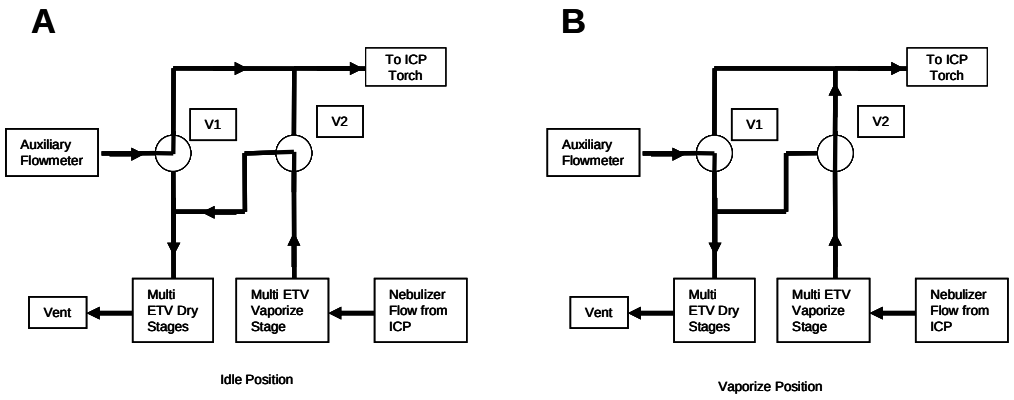

Figure 4.3: Gas routing diagrams for controlling the gas flow through the central channel of the ICPMS and the dry stages of the multiplexed ETV. V1 is an Asco (Dallas, Tx) Model 8320G43 three-way valve and V2 is a Burkert (Irvine, Ca) model 0311 three-way valve.

There are two valve positions that are needed during the operation of the multiplexed ETV. The "Idle Position" is used when the multi ETV is either not in use, loading or rotating the vaporizer platform. The "Vaporize Position" is used only when the multi ETV is ready to vaporize a sample. In brief, all filament cells are continually

bathed in Ar and with caps to the ETV cells put in place, the Ar sheath gas to the vaporization cell flows through the cell and then through the transport tubing to the ICP.

4.3.5 Vaporizer Preparation

A length of braid was first soaked overnight in 4M HNO_3 to remove surface contamination. Once mounted in the braid holders, the braids were fired at normal vaporization temperature (32 VAC) several times to further remove contamination. When first heated, the braids would smoke for several seconds; however, no smoke was seen in subsequent heating cycles. Carbon braid is often used for valve seats and pump gaskets in high temperature or harsh environments. The addition of lubricants and/or incomplete graphitization of the starting material during fabrication would be beneficial to those end uses, but could result in "smoke" during pyrolysis or inefficient graphitization at the high temperatures used during ETV conditioning.

Because of the flexibility of the braid as received, it was easy to work with but could not be precisely positioned so the autosampler would reproducibly deposit the sample in the center of the loop of the braid for each cell. Fortunately, high temperature heating in the ETV holder significantly increased the degree of graphitization and consequently produced rigidity of the previously flexible braid. Thus, by precisely positioning each graphite loop relative to the autosampler during graphitization, the braid could be permanently positioned so the autosampler could reproducibly deposit sample in the same location on each braid. A narrow (*ca*. 3 mm), high purity graphite rod (see Figure 4.4) with a V-shaped groove was used to hold the braid in position while 40 VAC was applied to heat and graphitize the braid.

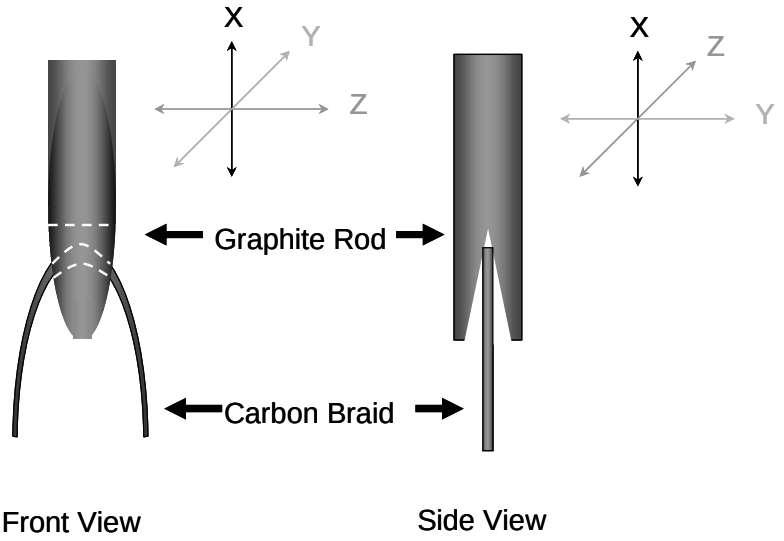

Figure 4: Conceptual drawing of the graphite rod used to align the braid. The loop of carbon braid fits into the V shaped notch of the graphite rod and is held in place as the braid is partial graphitized.

After heating, the braid took on a glossier gray appearance, indicating a change in the braid's structure. Subsequent vaporizations performed with an applied voltage of 32 VAC did not distort the shape of the braid.

4.4 FIGURES OF MERIT

4.4.1 Signal Shape and Characteristics

The signal shape of the multiplexed ETV braid vaporizer is compared with the tube-type furnace signal in Figure 4.5.

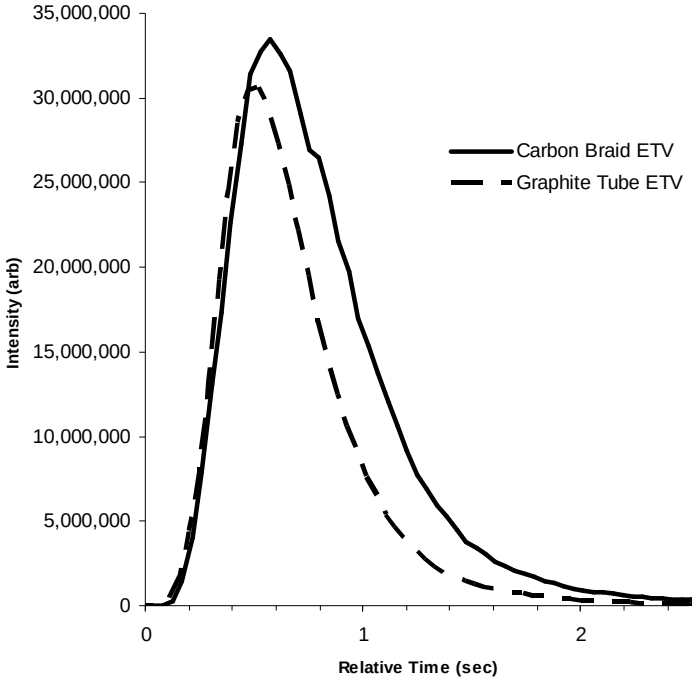

Figure 4.5: Peak comparison between the multiplexed ETV and graphite tube furnace ETV. The sample consisted of 5 µL of 100µg/L multimetal solution. Both peaks are of $^{115}In^{+}$ and plotted on the same relative time axis for comparison only. The area under the carbon braid ETV peak is 37% larger than the area under the graphite tube ETV peak.

The peaks have been offset along the time axis to coincide with the signal onset. The broadening of the peak utilizing the braid is likely a result of the dead volume (*ca.* 8 mL) of the ball joint cap of the multiplexed ETV system, which is larger than the original design used with the W filaments[5] in order to accommodate the taller carbon braid. While the peak height for the braid is *ca.* 10% higher than the tube-type ETV, the area is 40% larger. The cause of the increase in signal is not certain; however, several possible explanations exist. Since the increase appears independent of ionization potential of the element, it might be assumed that the increased carbon in the plasma is not increasing the ionization efficiency as was suggested previously for carbon-loading of a plasma [13, 14]

However, the increase in carbon from the braid may act as a physical carrier, or the *ca.* 8 mL volume in the chamber above the braid chamber may minimize condensation and loss of gaseous analyte that has been theorized to occur at the end cones with a end streaming graphite tube design[15].

4.4.2 Background Species

Figure 4.6 shows that the background spectrum from the carbon braid atomizer using 5 μL of a 1% HNO_3 solution is greatly reduced when compared to that seen previously with the W filaments.

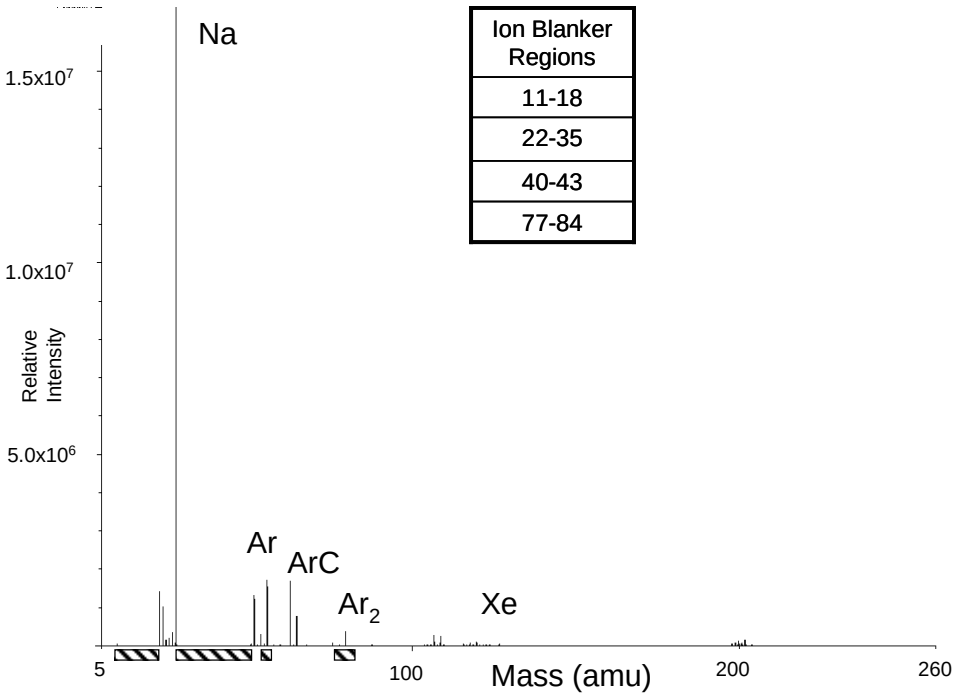

Figure 4.6 A full mass scan (5-250 amu) of a blank firing of the carbon braid vaporizers. Several contaminates are abundant, but are the results of instrument contamination or common plasma created polyatomics. The mass regions that are suppressed by the SmartGate® ion blanker are shown in the table and marked below the mass axis by hashed areas. These regions will have greatly suppressed signals and is shown to explain the suppressed argides and absence of atmospheric gases.

Since the TOF sends all ions down the flight tube, the Optimass utilizes an ion blanker to remove high flux ions of the analyst's choosing which might impact the detector lifetime.[16] The regions affected by the ion blanker are shown in Figure 4.6 and generally block peaks resulting from air entrainment, Ar^+ and major ArX^+ polyatomics. Even with ion blanking, several background species not inherent to the carbon braids are present. Several argide species (*e.g.*, Ar^+, Ar_2^+) are formed in the plasma, independent of braid usage. The peaks from Sn and Hg were contaminants in the mass spectrometer at the time of this study, Na is from sample contamination and Xe is

present in the liquid Ar that is used as the plasma gas. The presence of these peaks is not a consequence of using the carbon braid vaporizer. The only significant peak that was a result of the carbon braid is ArC^+. The ion blanker attenuated the signal for $^{24}C_2^+$ and $^{28}CO^+$ resulting in absence of these peaks.

4.4.3 Throughput and Performance

The typical tube-type ETV has a throughput of 20-30 sample/h, despite the vaporization phase only lasting 1-10 s. This limitation is from the serial completion of the loading, drying, thermal pretreatment, vaporization, cleaning and cooling stages. The multiplexed ETV performs these steps in parallel and is able to vaporize samples approximately 5 times faster (*ca.* 30s per determination or over 100 sample/h). An example of the throughput of the multiplexed ETV is shown in Figure 4.7, with 5 samples sequentially vaporized in *ca.* 150 s.

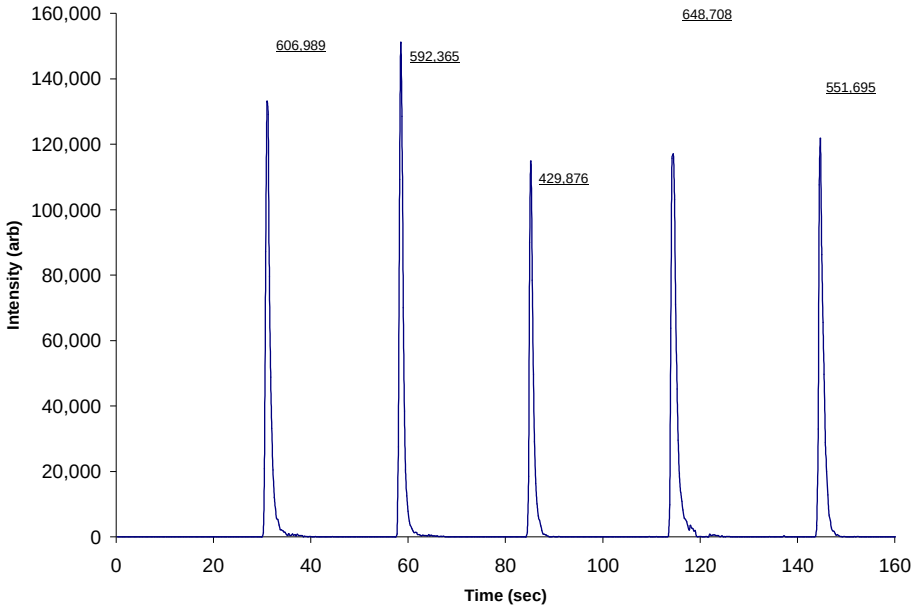

Figure 4.7 Five sequential vaporizations of 5 µL aliquots of 100 µg/L of multi metal solution, with the peaks below representing $^{115}In^{+}$. The areas for the peaks are listed and have a RSD of 15%.

While the previous study of the multiplexed ETV using W filaments required only *ca.* 20 s per determination[5], the current limitation is not on the multiplexed ETV but on the requirements of the ICP. When the gas valves are toggled (see Figure 4.3) the change in resistance to flow and the subsequent adjustment by the mass flow controller causes a pressure change. This requires *ca.* 10-15 s for the plasma to settle before vaporization can occur.

To examine the changes that occur with age, the braids were fired many times following the schedule listed in Table 4.1.

Vaporization #	Type of Measurement	Total Number of Firing	Conc. Of Metal Solution (µg/L)
1-6	Cleaning and Preparation	60	--
7-9	Blank	30	0
10	Calibration Curve	10	5
11	Calibration Curve	10	10
12	Calibration Curve	10	50
13-14	Samples	20	50
15	Samples	10	100
16-18	Blank	30	0
19	Calibration Curve	10	5
20	Calibration Curve	10	10
21	Calibration Curve	10	50
22-23	Samples	20	50
24	Sample	10	100
25-27	Blank	30	0

Table 4.1: Schedule of samples used for aging study of the carbon braid vaporizers.

To gauge the effects of aging on the braids, the integrated signal from each firing was divided by the concentration of the sample to obtain the sensitivity in units of L/µg of analyte. This method made it possible to directly compare samples of different concentrations. It should be noted that the sensitivity decreased with the increasing number of vaporizations for all of the elements used in this study. To compare the different elements, the percent change of the sensitivity was calculated with and without the benefit of $^{115}In^{+}$ as an internal standard. An example of $^{75}As^{+}$ is shown in Figure 4.8.

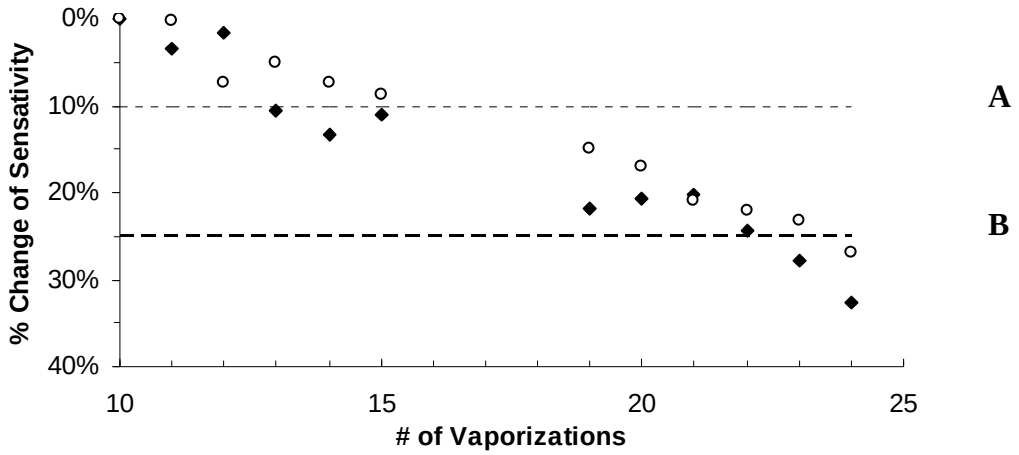

Figure 4.8: An example of the change in sensitivity as a function of number of vaporizations for one of the elements studied (*e.g.*, $^{75}As^{+}$) both with $^{115}In^{+}$ as an internal standard (open circles) and without an internal standard (closed diamonds). The dotted line (**A**) marks a 10% decrease in sensitivity and the dashed line (**B**) marks a 25% decrease in initial sensitivity.

The values for the 10% and 25% points are in Table 4.2. The sensitivity of the refractory elements decreases the quickest, while more volatile elements change more slowly. The schedule on Table 4.1 shows a total of 27 vaporizations per braid, which includes 9 blanks and 6 preparatory firings. The average minimum lifetime a braid is *ca.* 30 firings, which is much lower than the lifetime of a tube-type furnace. When one braid breaks, it must be replaced before the analysis can continue because of the parallel circuits used in many of the stages. While this is a low lifetime per *braid*, the lifetime of the entire 10 braids multiplexed ETV is 300 vaporizations, which compares favorable with the 200 use lifetime of a tube type furnace.

	Sensitivity Change (Vaporization #)			
	Without Internal Standard		With $^{115}In^{+}$ Internal Standard	
	10% Decrease	25% Decrease	10% Decrease	25% Decrease
^{7}Li	14	19	19	24
^{9}Be	12	15	14	19
^{27}Al	13	19	15	23
^{50}Cr	13	19	14	19
^{51}V	15	20	19	24
^{55}Mn	13	19	15	22
^{57}Fe	13	19	15	22
^{59}Co	14	22	18	24
^{60}Ni	13	14	15	19
^{63}Cu	14	21	19	23
^{66}Zn	14	20	20	23
^{69}Ga	12	19	19	22
^{74}Ge	13	19	19	22
^{75}As	13	23	19	24
^{85}Rb	14	23	19	24
^{88}Sr	13	20	15	22
^{107}Ag	13	21	19	22
^{114}Cd	13	21	19	23
^{115}In	13	21	19	23
^{133}Cs	15	23	19	24
^{138}Ba	13	15	15	19
^{205}Tl	15	21	19	24
^{208}Pb	15	22	19	24
^{209}Bi	14	21	19	24
^{238}U	12	13	15	19

Table 4.2: The vaporization that yielded a decrease in sensitivity of 10% and 20% are shown. These points can be used to estimate the rate of sensitivity change for each element. All of the element's signals decreased with increasing number of firings.

4.4.4 Oxygen Ashing

Oxygen ashing is a technique that can be used to remove combustible material (such as biological and other organics) from a sample by reaction with oxygen. Oxygen

ashing was first suggested as a general means of removing organic material *via* combustion on the atomizer for ETAAS by Kundu and Pevot[17], and it has become commonplace in ETAAS, as well as having been applied to ETV-ICPMS. The sensitivity of W to oxidation made oxygen ashing impossible when using the W filaments of the previous multiplexed system.

To characterize the carbon braid performance with oxygen ashing, a 0.1% bovine serum albumin (BSA) solution was prepared in DI water with compressed air as the oxygen source. No char, ash or smoke was visible after repeated ashings of BSA. The small amount of BSA added to the braid may have made a visual determination of accumulation difficult. A 100 mL aliquot of the 0.1% BSA solution was spiked with 100 µL of 10 mg/L multimetal solution, for an overall concentration of 10 µg/L of various metals. The results of the analysis for the spiked BSA solution were compared to those from a 1% HNO_3 solution to evaluate recoveries, and the results are summarized in Table 4.3. The average recovery of the elements listed is 96±17%, which is similar to results from of other biological material[18-21].

	Oxygen Ashing Analyte Recovery
^{7}Li	92%
^{9}Be	79%
^{27}Al	87%
^{50}Cr	104%
^{51}V	104%
^{55}Mn	104%
^{57}Fe	84%
^{59}Co	98%
^{60}Ni	115%
^{63}Cu	116%
^{66}Zn	91%
^{69}Ga	121%
^{74}Ge	91%

	Oxygen Ashing Analyte Recovery
^{75}As	120%
^{85}Rb	99%
^{88}Sr	107%
^{107}Ag	86%
^{114}Cd	114%
^{115}In	89%
^{133}Cs	89%
^{138}Ba	74%
^{205}Tl	87%
^{208}Pb	103%
^{209}Bi	103%
^{238}U	42%

Table 4.3: A comparison of the recoveries of elements in a BSA solution compared to a solution without biological material. Oxygen ashing was used to remove the biological material, reducing the interference caused by the BSA.

4.4.5 Precision

To measure precision, RSD values (N=20) were calculated for a suite of metals.as shown in Figure 4.9. In Figure 4.9, the grey bars indicate the RSD for the elements using the internal standard $^{115}In^{+}$, the open circles are the RSD values without an internal standard and the closed diamonds are the appearance temperatures[22]

The precisions for the multiplexed ETV are higher than those expected using a graphite tube-type ETV, which are typically <10%. The use of ^{115}In as an internal standard improved the precision for several elements (*e.g.,* $^{50}Cr^{+}$, $^{60}Ni^{+}$, $^{66}Zn^{+}$, $^{74}Ge^{+}$, $^{85}Rb^{+}$, $^{88}Sr^{+}$, $^{138}Ba^{+}$ and $^{205}Tl^{+}$) but also decreased the precision of a few elements (*e.g.*, $^{51}V^{+}$, $^{55}Mn^{+}$ and $^{238}U^{+}$). Other elements (*e.g.,* $^{59}Co^{+}$, $^{69}Ga^{+}$, $^{133}Cs^{+}$ and $^{138}Ba^{+}$) were also evaluated as internal standards, but $^{115}In^{+}$ gave the overall best performance for the suite

of elements used in this study. There also appears to be no trend regarding precision's dependence on analyte volatility.

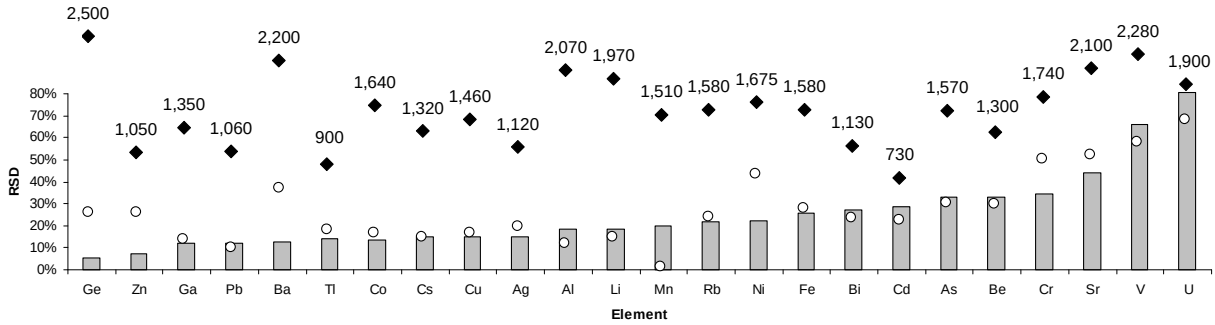

Figure 4.9: Graph of RSD values by element with the aid of $^{115}In^{+}$ as a internal standard (grey bars) and without an internal standard (open circles). Appearance temperatures [22] (closed diamonds) with the corresponding temperature value (in K) are also shown. Be, Tl and U appearance temperatures are estimates.

If the set of vaporizers is studied as 10 individual vaporizers, instead of an ensemble, the RSD values for the braids were found to be *ca.* 10%. This is an improvement over the RSD values found for the ensemble. However, to gain this advantage, each braid would require a separate calibration curve. While this would result in a gain in precision, the result would be a loss of the multiplexed advantage.

There are many possible reasons that the RSD values for the braid vaporizers are much higher than a conventional tube-type furnace. The apex of the loop of carbon braid (see Figure 4.2), which should be the hottest part of the braid, becomes visibly thinner as the braid ages, likely as a result of carbon sublimation and oxidation of this high surface area material. As the braid thins, the overall resistance increases. The increase in

resistance causes a decrease in the amount of power dissipated in the braid at a constant voltage but an increased power density in the thinning center. Thus, the temperature gradient from the center to the ends of the braid becomes more steep. It is expected that analyte movement away from the center, either by capillary action of the deposited liquid or vaporization/condensation during heating, will experience different heating conditions from braid to braid and as any individual braid ages. This can include differences in temperature as a function of the distance traveled as well as changes in the composition of the carbon (*e.g*, number of active carbons.). This problem is further exacerbated by the non-uniform heating of the braid, even across the braid diameter. Deposition of a pyrolytic surface on the carbon braid should minimize sample wetting of the surface. However, wetting still occurs, especially as the solution temperature is raised during drying.

4.4.6 Detection Limits

Detection limits are listed in Table 4.4 for several elements. Detection limits were calculated using S/N=3, where N is calculated from the standard deviation of 30 blanks and the LODs are extrapolated from the slope of the calibration curve. Overall, detection limits are higher than those of the tube-type ETV. The refractory metals ($^{9}Be^{+}$, $^{60}Ni^{+}$ and $^{27}Al^{+}$) have higher detection limits than the tube-type furnace probably due to lower sensitivities caused by lower vaporization temperatures achievable by the braid and/or the thermal gradient discussed previously. Other metals ($^{114}Cd^{+}$, $^{59}Co^{+}$, $^{133}Cs^{+}$, and $^{69}Ga^{+}$) showed reasonable sensitivities, but suffered from memory effects which contributed to a higher standard deviation of the blank.

	Detection Limits			
	Multi ETV		Tube Type ETV	
	µg/L	pg	µg/L	pg
^{7}Li	2.4	12	0.350	3.50
^{9}Be	20	100	0.056	0.558
^{27}Al	3.1	15	0.169	1.69
^{50}Cr	18	92	0.372	3.72
^{51}V	18	88	0.030	0.301
^{55}Mn	0.30	1.5	0.030	0.297
^{57}Fe	12	59	0.885	8.85
^{59}Co	7.4	37	0.009	0.94
^{60}Ni	10	50	0.090	0.896
^{63}Cu	3.0	15	0.122	1.22
^{66}Zn	200	900	0.182	1.82
^{69}Ga	4.4	22	0.017	0.169
^{74}Ge	0.71	3.5	0.075	0.756
^{75}As	0.17	0.085	0.129	1.30
^{85}Rb	19	96	0.015	0.148
^{88}Sr	1.1	5.7	0.034	0.340
^{107}Ag	2.5	12	0.040	0.400
^{114}Cd	7.2	36	0.035	0.353
^{115}In	0.44	2.2	0.030	0.297
^{133}Cs	7.1	35	0.050	0.497
^{138}Ba	2.7	14	0.045	0.452
^{205}Tl	0.79	0.40	0.021	0.210
^{208}Pb	7.7	38	0.041	0.408
^{209}Bi	0.29	1.5	0.122	1.22

Table 4.4. Comparison of detection limits for the Multiplex ETV and graphite tube ETV

4.5 CONCLUSION

By replacing the W filament vaporizers of the multiplexed ETV system with carbon braids, background levels were reduced due to the lower impurity levels in the carbon braids. The change in material also permitted oxygen ashing, which would

expand the sample types that can be used with this system (*e.g.*, biological samples). The precisions were within approximately 30% (RSD) which may be adequate for some analytical situations where throughput is important. Precision for refractory elements was even poorer and had an average RSD of 60%. These precisions compare unfavorably with more conventional graphite tube-type ETVs where precisions of <10% are expected.

When used at *ca.* 2800^{o}C vaporization temperatures, the average minimum filament lifetime is not outstanding even though use in the 10-braid multiplex system yields 300 analyses before a filament change is needed. The lifetime increases substantially if the vaporization temperature is lowered, *i.e.*, lowering the voltage from 32VAC to 24VDC doubled the lifetime of the braids, but had a detrimental effect on the signals produced by the refractory elements.

The multiplexed ETV system with the carbon braids retained many of the desirable features of an ETV introduction system, *i.e.*, microanalytical capabilities, complex matrix handling, *etc*. The change from W to C as the vaporizer material produced the primary objective of reducing background levels and permitting oxygen ashing. However, lifetime and precision needs improvement, perhaps through the use of another form of carbon besides braided material. Similarly, it would be ideal to focus the power into a less lengthy but equally massive vaporizer to minimize the effects of mass loss during high temperature heating which, in turn, should significantly improve the lifetime. A lower surface area atomizer might further reduce thermal degradation and minimize the analyte-vaporizer interactions that could lead to incomplete vaporization of refractory materials.

4.6 ACKNOWLEDGEMENTS

This research was supported by the National Science Foundation (Grant number CHE-0315336), and GBC Scientific Equipment. TEK would like to thank the Robert A. Welch Foundation for a summer fellowship. The authors would like to thank the UT Chemistry Machine Shop and Glass Shop for helpful suggestions.

REFERENCES

[1] Kirkbright, G.F. and A.F. Ward, *Atomic emission spectrometry with an induction-coupled high frequency plasma source. Comparison with the inert-gas shielded premixed nitrous oxide-acetylene flame for multielement analysis.* Talanta, 1974. **21**(11): p. 1145-65.

[2] Stewart, I.I. and J.W. Olesik, *Transient acid effects in inductively coupled plasma optical emission spectrometry and inductively coupled plasma mass spectrometry.* J. Anal. At. Spectrom., 1998. **13**(9): p. 843-854.

[3] Denoyer, E.R., A. Stroh, and Q. Lu, *High sample throughput with rapid microsampling flow injection ICP-MS.* At. Spectrosc., 1993. **14**(2): p. 55-9.

[4] Dean, J.R., et al., *Characteristics of flow injection inductively coupled plasma mass spectrometry for trace metal determination.* J. Anal. At. Spectrom., 1988. **3**(2): p. 349-54.

[5] Venable, J.D., M. Detwiler, and J.A. Holcombe, *Multiplexed electrothermal vaporization sample introduction system for inductively coupled plasma spectrometry.* Spectrochim. Acta, Part B, 2001. **56B**(9): p. 1697-1706.

[6] Montaser, A. and S.R. Crouch, *New methods for programmed heating of electrically heated nonflame atomic vapor cells.* Anal. Chem., 1975. **47**(1): p. 38-45.

[7] Montaser, A., S.R. Goode, and S.R. Crouch, *Graphite braid atomizer for atomic absorption and atomic fluorescence spectrometry.* Anal. Chem., 1974. **46**(4): p. 599-601.

[8] West, T.S. and X.K. Williams, *Atomic absorption and fluorescence spectroscopy with a carbon filament atom reservoir. I. Construction and operation of atom reservoir.* Anal. Chim. Acta, 1969. **45**(1): p. 27-41.

[9] Langer, D. and J.A. Holcombe, *Thermophoretic Collection and Analysis of Submicrometer Ag Particles Emitted from a Graphite Tube-Type Electrothermal Vaporizer.* Anal. Chem., 1999. **71**(3): p. 582-588.

[10] Touloukian, Y.S. and D.P. DeWitt, *Thermal Radiative Properties: Nonmetallic Solids (Thermophysical Properties of Matter, Vol. 8).* 1972. 1763 pp.

[11] Campbell, I.E. and Editor, *High Temperature Technology*. 1956. 526 pp.

[12] Kozlov, B., A. Saint, and A. Skroce, *Elemental fractionation in the formation of particulates, as observed by simultaneous isotopes measurement using laser ablation ICP-oa-TOFMS.* J. Anal. At. Spectrom., 2003. **18**(9): p. 1069-1075.
[13] Tan, S.H. and G. Horlick, *Matrix-effect observations in inductively coupled plasma mass spectrometry.* J. Anal. At. Spectrom., 1987. **2**(8): p. 745-63.
[14] Venable, J.D. and J.A. Holcombe, *Signal enhancements produced from externally generated 'carrier' particles in electrothermal vaporization-inductively coupled plasma mass spectrometry.* Spectrochim. Acta, Part B, 2000. **55B**(7): p. 753-766.
[15] Holcombe, J.A. and G. Ertas, *Monte Carlo simulation of transport from an electrothermal vaporizer.* Spectrochim. Acta, Part B, 2006. **61B**(6): p. 743-752.
[16] GBC Scientific Equipment Pty. Ltd.,. (2006). *A time of flight mass spectrometer*. 2005-AU14612006034530.
[17] Kundu, M.K. and A. Prevot, *Oxygen-rich atmosphere for direct determination of copper in oils by nonflame atomic absorption spectrometry.* Anal. Chem., 1974. **46**(11): p. 1591-5.
[18] Beres, S., R. Thomas, and E. Denoyer, *the benefits of electrothermal vaporization for minimizing interferences in ICP-MS.* Spectroscopy (Duluth, MN, United States), 1994. **9**(1): p. 20-6.
[19] Fonseca, R.W. and N.J. Miller-Ihli, *Analyte transport studies of aqueous solutions and slurry samples using electrothermal vaporization ICP-MS.* Appl. Spectrosc., 1995. **49**(10): p. 1403-10.
[20] Fonseca, R.W., et al., *Effect of oxygen ashing on analyte transport efficiency using ETV-ICP-MS.* Appl. Spectrosc., 1997. **51**(12): p. 1800-1806.
[21] Miller-Ihli, N.J. and S.A. Baker, *Microhomogeneity assessments using ultrasonic slurry sampling coupled with electrothermal vaporization isotope dilution inductively coupled plasma mass spectrometry.* Spectrochim. Acta, Part B, 2001. **56B**(9): p. 1673-1686.
[22] L'Vov, B.V., *Electrothermal atomization - the way toward absolute methods of atomic absorption analysis.* Spectrochim. Acta, Part B, 1978. **33B**(5): p. 153-93.

Chapter 5: Conclusions and Future Directions

5.1 CONCLUSIONS

The less than commonplace use of ETV as a popular, alternative sample introduction technique may result from the technique's shortcomings, perceived or actual. The inherent benefits of ETV sample introduction (*e.g*, µL sample size, salt tolerance, solid sampling, thermal separation, oxygen ashing, *etc*) are sometimes over shadowed by other analytical concerns (*e.g.*, low sample throughput, lack of commercial instrumentation, complexity of thermal programming, *etc*). These must be overcome or, at least clarified, in order to increase the acceptance of ETV as a sample introduction technique for ICPMS.

The addition of carbon braids to the multiplexed ETV is an upgrade to the original device[1]. The upgrade maintains the modest power requirements (~300W) and high throughput (*ca.* 120 samples/h), while reducing background and adding the ability to perform oxygen ashing. The latter capability would not have been possible with the W filaments due to the ease of metal filament oxidation The advantages of the carbon braid come at the price of poorer precision for the refractory elements (*e.g.*, RSD values *ca.* 60%). The lifetime of each braid is *ca.* 30 vaporizations, which is much lower than the 200+ expected from a tube-type furnace. However, with the 10 braids in the multiplexed ETV, this allows for 300 vaporizations before the braids have to be replaced.

The addition of a glass "T" to the spray chamber allows the use of an ETV in addition to a nebulizer. Instead of using the ETV to *replace* a nebulizer, an ETV can be used to *augment* the information available from a nebulizer. While some performance

characteristics of the ETV are reduced with the glass T when compared to a stand-alone ETV, the ETV add-on does not affect the performance of the nebulizer. Polyatomic interferences formed in the plasma (*e.g.*, $^{75}ArCl^{+}$ and $^{75}As^{+}$) could be separated and quantified using the ETV and with superior detection limits than using a nebulizer alone.

5.2 FUTURE DIRECTIONS

Instrument manufacturers are constantly pushing to make instruments less expensive, faster and more sensitive. Recent advances in time of flight mass spectrometer (TOFMS) design for ICP have made an excellent compliment to the analysts who have transient signal acquisition needs [2, 3]. The near simultaneous nature of TOFMS signal acquisition removes spectral skew, a misrepresentation of a transient peak due to scanning multiple masses, which can occur with scanning type mass spectrometers when measuring fast transient signals. This can alter the performance of ETV determination depending on the number of elements monitored[4, 5]. A byproduct of the simultaneous signal acquisition is a reduction in analysis time (and cost) when determining many elements in a given sample. This makes ICP-(TOF)MS an excellent choice for monitoring many masses using a transient signal. Unfortunately, TOF-based instruments are currently less popular than quadrupole-based instruments, possibly as a consequence of the lack of widespread availability of commercial instruments until recently. The obvious compatibility of the ICP(TOF)MS with the ETV may combine with past advantages of ETV introduction along with other analytical advantages suggested in this thesis may have a very positive effect of the adoption of ETV as an

analytical technique as a more direct means of solving complex analytical problems involving ultratrace and microtrace analysis.

REFERENCES

[1] Venable, J.D., M. Detwiler, and J.A. Holcombe, *Multiplexed electrothermal vaporization sample introduction system for inductively coupled plasma spectrometry.* Spectrochim. Acta, Part B, 2001. **56B**(9): p. 1697-1706.

[2] Hieftje, G.M., et al., *Toward the next generation of atomic mass spectrometers.* J. Anal. At. Spectrom., 1997. **12**(3): p. 287-292.

[3] Sturgeon, R.E., J.W.H. Lam, and A. Saint, *Analytical characteristics of a commercial ICP orthogonal acceleration time-of-flight mass spectrometer (ICP-TOFMS).* J. Anal. At. Spectrom., 2000. **15**(6): p. 607-616.

[4] Resano, M., et al., *Evaluation of the multi-element capabilities of electrothermal vaporization quadrupole-based ICP mass spectrometry.* J. Anal. At. Spectrom., 2001. **16**(9): p. 1018-1027.

[5] Venable, J.D., D. Langer, and J.A. Holcombe, *Optimizing the Multielement Analysis Capabilities of an ICP Quadrupole Mass Spectrometer Using Electrothermal Vaporization Sample Introduction.* Anal. Chem., 2002. **74**(15): p. 3744-3753.

Appendix A

A.1 Design Changes to the Multiplex ETV

A.1.1 Electrical Design

A.1.1.1 Overview

Modifications were made to vaporization and ashing stages' power handling system to accommodate the addition of the carbon braids. The transistor based circuit for the vaporize stage was disconnected, but still resides on the Filament Power Board for future use. The power supply for the vaporize stage is a Variac® autotransformer, which can provide in excess of 1,000W of power. The re-designed system uses relays to control the power delivery to the filaments, which isolate the filaments from the power supplies.

A.1.1.2 Vaporizer Stage Power Supply

The Variac® autotransformer is used as a variable power supply to power the vaporizers. The power draw of the Variac® is low enough to allow the Variac® to be plugged into the 110 VAC outlets on the multiplexed ETV. One end of thean autotransformer is at the neutral potential, while the other end is hot. To prevent the development of a dangerous situation where the power leads switched (*i.e.* using a non-polarized plug), the relay circuit (shown in Figure A.1) was designed to float. The Variac® can be replaced with any power supply without a need for modification. The power from the Variac® is carried to a daughter board (located near the Filament Power Board at the rear of the instrument) *via* 3 pairs of a shielded cable. The shielding is unnecessary for this application, but the cable was convenient for attaching to the daughter board. The pairs are attached to the wiper of two relays on the daughter board and the NC terminal is connected to the vaporization station. The replays are controlled

by a simple transistor circuit that sources current for the coils. A 5V signal is sent from LabView® on Pin32 of the DAQ output card to the base of a transistor.

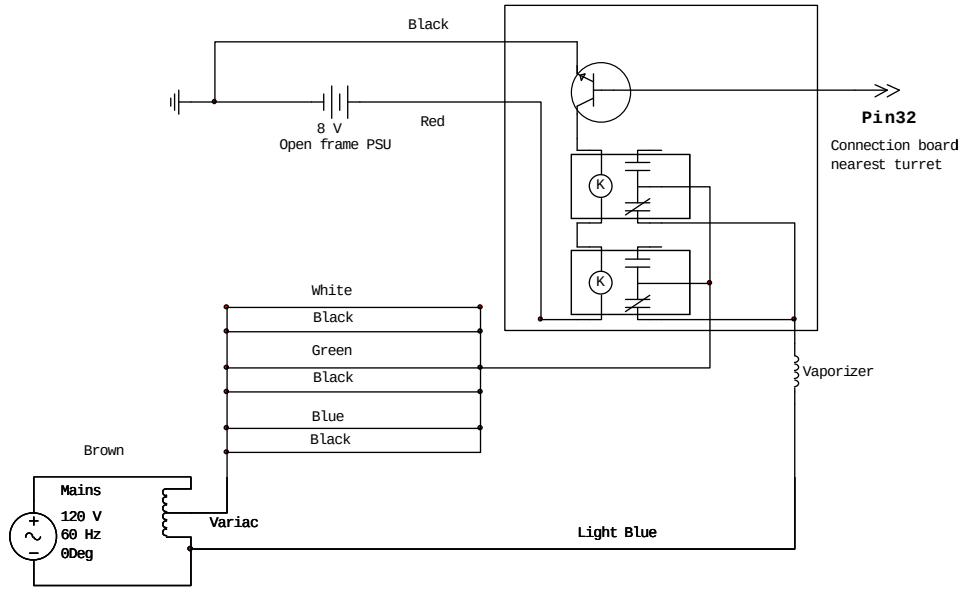

Figure A.1: Schematic representation of the modified vaporizer stage circuit for the multiplexed ETV.

The transistor saturates, sourcing power from an 8VDC supply. This closes the relays, allowing the Variac® to heat the vaporizer filament.

A.1.1.3 Ash Stage Power Supply

The power supply for the ash stage was originally fabricated in the original, W filament based multi ETV, but never connected. The input power was increased to 24 VDC from the 7.5 VDC in the original design. The upgrade only required moving the electrical connections and temperature set points on the Filament Power Board and in LabView®.

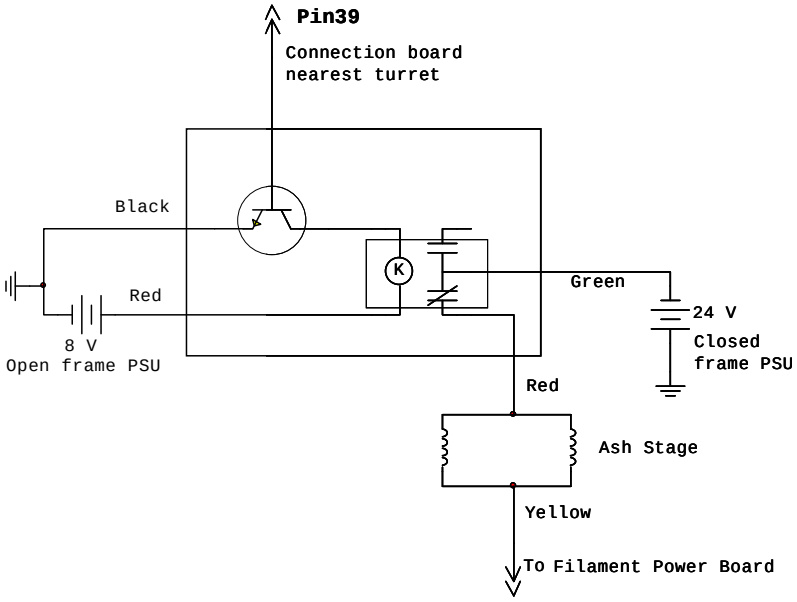

Figure A.2: Schematic representation of the modified ash stage circuit for the multiplexed ETV.

The redesigned ash stage control (Figure A.2) added a relay to prevent accidental heating of the ash stage, due to bridging (*e.g.*, connections between adjacent stages) during rotation. The configuration is similar to the one used for the vaporization stage (Figure A.1). The relay system is floating so that the transistor controlled power delivery can be replaced at anytime with a different power source. The temperature for the ash stage is set in the LabView® program that operates the multiplex ETV. The default temperature setting is 800 ºC, but is capable of higher temperatures.

VITA

Thomas Eugene Kreschollek was born in New Haven, Connecticut on October 2, 1979 to Marjorie and William Kreschollek. He attended Guilford High School, in Guilford, Connecticut. After graduation, he escaped to Henderson State University, in scenic Arkadelphia, Arkansas. He earned in Bachelor of Science degree with a major in chemistry in May 2002. In August 2002 he entered into the doctorial program at the University of Texas in the field of analytical chemistry.

Permanent address: 8244 Magnolia Village Dr, Mobile, Al 36695

This dissertation was typed by the author.